Chem Soc Rev

ROYAL SOCIETY OF CHEMISTRY

REVIEW ARTICLE

View Article Online
View Journal | View Issue

Cite this: *Chem. Soc. Rev.*, 2021, **50**, 5631

Fundamental studies to emerging applications of pyrrole-BF_2 (BOPHY) fluorophores

Aisha N. Bismillah * and Ivan Aprahamian *

Received 1st February 2021

DOI: 10.1039/d1cs00122a

rsc.li/chem-soc-rev

BF_2-based fluorophores, such as the well-known BODIPY (4,4-difluoro-4-bora-3*a*,4*a*-diaza-*s*-indacene) dye, are prevalently used in diverse research areas (*e.g.*, bioimaging and chemosensing) as they exhibit promising features including high quantum yields, fine-tuned absorption and emission spectra as well as good photostability and biocompatibility. While BODIPY dyes are most commonly used in such applications, other BF_2-based fluorophores, such as BOPHY (bis(difluoroboron)-1,2-bis((1*H*-pyrrol-2-yl)methylene)hydrazine – which possess their own characteristic features – are rising in popularity and are being used in a range of applications spanning from molecular sensors to photosensitizers for solar cells. This review examines select examples of BOPHY dyes to highlight the progression of their development while detailing their syntheses and photophysical properties including structure–property relationships. Applications of a number of substituted BOPHYs made by the methods described in this review are also presented.

1. Introduction

Organic fluorescent dyes are indispensable and powerful tools at the disposal of scientists investigating chemical, physical, biological events and processes. The chemical and structural versatility of organic chromophores such as coumarins,[1] naphthalimides,[2] fluoresceins,[3] and others[4–8] allow for the fine tuning of properties (*e.g.*, Stokes shifts, emission quantum yields (Φ_f), absorption, and emission spectra) to accommodate important and particular functions. It is no wonder then that these chromophores are used in a diverse array of applications which range from biological probes,[9–12] molecular sensors,[13–16] and fluorescent markers[17] to light harvesting agents,[18] organic light-emitting diodes,[19] and optoelectronic device components.[20–23] Among all the synthetic fluorophores with tunable photophysical properties, tetracoordinated BF_2-hybrid complexes of π-conjugated chelates occupy a privileged position because of their ease of synthesis, high chemical and photochemical stability as well as

Department of Chemistry, Dartmouth College, Hanover, New Hampshire 03755, USA. E-mail: aisha.n.bismillah@dartmouth.edu, ivan.aprahamian@dartmouth.edu

Aisha N. Bismillah

Aisha Bismillah obtained her MChem degree from the University of Central Lancashire in 2015. She received her PhD degree from the University of Durham in 2019 working under the tutelage of Asst. Prof. Paul McGonigal where her research focused on fluxional carbon cages and their 'shapeshifting' properties. She is currently training as a postdoctoral researcher in the Aprahamian group at Dartmouth College under a US–UK Fulbright Scholarship. Aisha's research focuses on hydrazone switch-based reaction cascades.

Ivan Aprahamian

Ivan Aprahamian received all his degrees (BSc – 1998, MSc – 2000, and PhD – 2005) from the Hebrew University of Jerusalem. His doctoral research was conducted under the supervision of Professors Mordecai Rabinovitz and Tuvia Sheradsky. He started his independent career at Dartmouth College in 2008, after finishing his postdoctoral research with Sir Fraser Stoddart (UCLA), and was promoted to Associate Professor with tenure in 2014, and Full Professor in 2019. Ivan is the recipient of numerous awards including the Cram Lehn Pedersen Award in Supramolecular Chemistry and a Humboldt Research Fellowship, and is a Fellow the Royal Society of Chemistry.

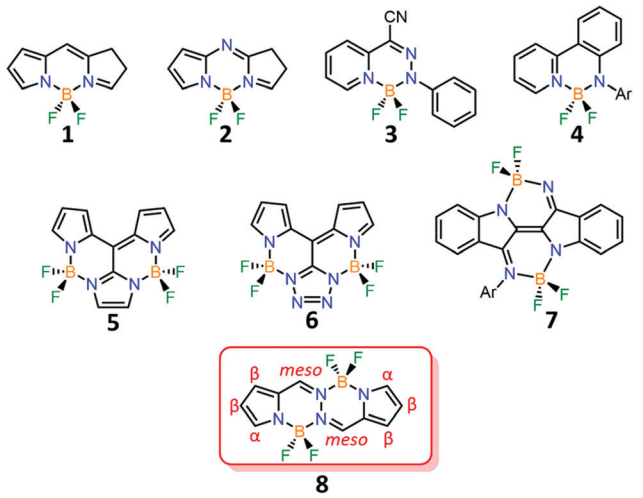

Fig. 1 The core skeletal structures of nitrogen–boron–nitrogen chelated BF_2 compounds derived from dipyrrin (**1**, BODIPY), *aza*-dipyrrin (**2**, *aza*-BODIPY), hydrazone (**3**, BODIHY), anilido pyridine (**4**), dipyrromethanes (**5**, BOIMPY), dipyrrin (**6**, *aza*-BOIMPY), indigo-*N*,*N*′-diarylamine (**7**) and hydrazine (**8**, BOPHY).

desirable photophysical properties. These characteristics have allowed BF_2 complexes to be used in data storage,[24] electrochromic devices,[25] photoconductors,[26] and as both *in vitro* and *in vivo* imaging agents,[27–29] photodynamic therapy devices,[30–32] as well as bioconjugated probes and immunoassay labels.[33–35]

One of the most well-documented boron-centered fluorophores is BODIPY (4,4-difluoro-4-bora-3*a*,4*a*-diaza-*s*-indacene) (**1**; Fig. 1),[9,36] with its versatile, readily accessible and easy to functionalize boron–dipyrrin skeleton. This structural adaptability of BODIPY allows for the fine-tuning of key (photo)physical properties, such as its molar extinction coefficient (ε), thermal resistance, photostability, and Φ_f.[9] Nonetheless, BODIPY dyes are limited by their weak emission in the solid state, which results from self-absorption as well as aggregation-induced emission quenching. Overall, these shortcomings present boundaries, impacting the applicability of these dyes, for example, when visualizing the cellular environment[37] or developing optoelectronic devices.[38] Although some studies have reported enhanced solid-state emission[39,40] through the addition of bulky substituents, or when merged with polymers, these approaches are only partially successful and can result in unwanted side effects (*e.g.*, changes in photophysical properties).[41] As a consequence of these limitations, in combination with the drive for new fluorescent scaffolds to enrich the pool of fluorophores for downstream applications, analogous architectures of BODIPY have been developed. Examples of such chromophores are ones derived from *aza*-dipyrrin (**2**, *aza*-BODIPYs),[42–45] hydrazones (**3**, BODIHY),[41,46] anilido pyridine (**4**),[47,48] dipyrromethanes (**5**, BOIMPYs),[49] dipyrrin (**6**, *aza*-BOIMPYs)[50] and indigo-*N*,*N*′-di-arylamine (**7**).[51] Moreover, other systems based on nitrogen–boron–oxygen bridges instead of the nitrogen–boron–nitrogen bridges found in BODIPY have also been developed.[52–54]

One of the more recently developed tetracoordinated BF_2 complexes is known as BOPHY (bis(difluoroboron)-1,2-bis((1*H*-pyrrol-2-yl)methylene)hydrazine) (**8**), which was first developed by Ziegler and coworkers in 2014.[55,56] This dye is based on pyrrole–boron difluoride and includes two BF_2 units. This BOPHY fluorophore has been quickly adopted by practitioners because of its promising properties (*e.g.*, high Φ_f values) which have directly led to applications in several sectors – pH sensing, ion detection, heterojunction solar cells and photocatalysts for hydrogen production. While this dye is closely related and somewhat similar in structure to BODIPY,[57] it possesses its own unique features, such as Φ_f values nearing unity and slightly higher Stokes shifts (although the substitution pattern must be taken into account). In this review, we highlight a series of publications showing the progression of the BOPHY dyes over the past few years, with a focus on their synthesis, spectroscopic characteristics, and emerging applications.

2. General synthesis and properties of the BOPHY core

The BOPHY core (Fig. 1) is comprised of four 5,6,6,5-tetracyclic rings: two pyrrole rings at the periphery and two six-membered rings in the middle, each containing a BF_2 moiety.[58] The fluorophore is rigidly planar, possesses an inversion center (C_{2h} symmetry), and has α-, β-, and *meso*-positions that can be functionalized. The general synthesis of BOPHY (Scheme 1) – which is also used to synthesize BOPHY **8** – starts with a formylated pyrrole.[56] Condensation with hydrazine hydrate in the presence of a catalytic amount of acetic acid provides the azine within an hour at room temperature. The addition of the Lewis acid boron trifluoride diethyl etherate, and either *N*,*N*-diisopropylethylamine or triethylamine as a base, yields the fluorophore after reacting for 24 hours. Slight variations in the synthetic procedure are required for compounds containing halogens – addition of the halogen group can either occur on the azine or after the BOPHY chromophore is formed.

The structures of the first BOPHYs synthesized **8** and **9** were elucidated *via* X-ray crystallography (Fig. 2). Analysis of the single crystals confirmed the presence of four rigid ring structures in the chromophore, two five-membered pyrrole units (where the dihedral angles are less than 2.7°), and two central BF_2-containing

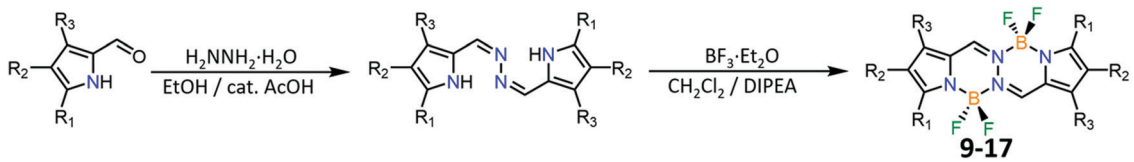

Scheme 1 General synthetic pathway for the BOPHY chromophores **9–17** starting from a formylated pyrrole.

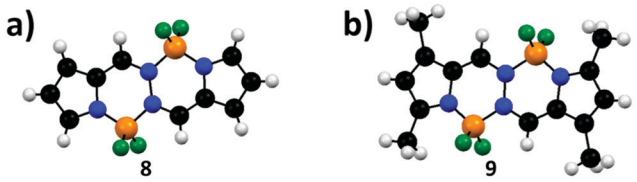

Fig. 2 X-Ray structures of BOPHY complexes **8** and **9** shown in ball and stick representations. Fluorine, boron, nitrogen, carbon, and hydrogen atoms are indicated by green, light orange, blue, black, and white respectively.

six-membered rings where only the fluorine atoms deviate from the plane. The crystal structures also show intramolecular C–H···F hydrogen bonds between the fluorine atoms and hydrogens atoms at the α- and *meso*-positions.[59]

Unfunctionalized BOPHY **8** exhibits two distinct absorption bands with maxima (λ_{max}) at 424 and 442 nm in dichloromethane (CH_2Cl_2), with molar extinction coefficients of 40 900 and 38 600 M^{-1} cm^{-1}, respectively (Fig. 3a and Table 1). The origin of these bands has been attributed to single photon processes, alluding to vibrational progression in the excited state.[56] These observations are corroborated by time-dependent density functional theory (TD-DFT) calculations, which reveal an energy difference (1.3 *vs.* 1.6 kcal mol^{-1}) between two geometries of **8** with C_2 and C_i symmetries.[60] These geometries arise when the boron atoms deviate from the central plane either in the same or opposite side, respectively. Compound **9** displays slightly red-shifted absorption bands with λ_{max} at 444 and 467 nm, and with similar extinction coefficients of 37 500 and 37 400 M^{-1} cm^{-1}. Both complexes exhibit two emission bands in solution (λ_{em} = 465 and 493 nm for **8**, and λ_{em} = 485 and 518 nm for **9**), with Φ_f in CH_2Cl_2 approaching unity (0.95 and 0.92 for **8** and **9**, respectively). The absorption and emission maxima of complexes **8** and **9** display only slight solvent dependency and have similar fluorescence lifetimes (2 ns) when compared against classical BODIPYs.[38] Solutions of **8** and **9** are stable towards light and air for days, and continuous irradiation of **8** in toluene with a 500 W xenon lamp shows excellent photostability with more than 98% of the compound remaining after an hour. The photostability was also demonstrated to be better than fluorescein in a dimethyl sulfoxide : water (1 : 1) mixture (Fig. 3b).[38]

Compounds **8** and **9** show strong fluorescence emission in the solid state and as thin films (Fig. 3c), whereas BODIPY dyes barely exhibit fluorescence in the solid state.[25] The absorption and emission bands are bathochromically shifted with respect

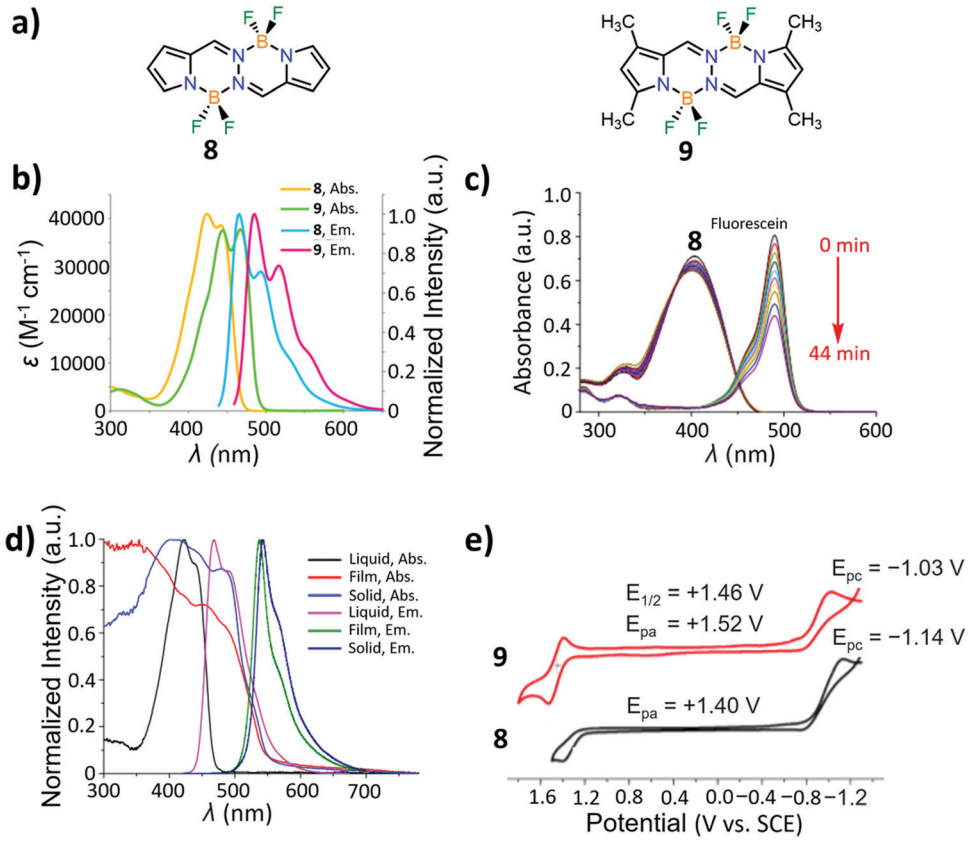

Fig. 3 (a) Chemical structures of BOPHYs **8** and **9**. (b) Absorption and emission spectra of **8** and **9** in CH_2Cl_2. (c) Photostability assessment of **8** (DMSO : H_2O, 1 : 1) relative to fluorescein (0.1 M NaOH solution) by absorbance monitoring during continuous irradiation with a 500 W Xe lamp over 44 minutes (30 mW cm^{-2}; >395 nm light used; 25 °C). (d) Normalized absorption and emission spectra of **8** in CH_2Cl_2, as thin films, and a solid powder. (e) CVs of **8** and **9** (1 mM) measured in a CH_2Cl_2 solution at 25 °C containing $TBAPF_6$ (0.1 M) as the supporting electrolyte, glassy carbon as the working electrode with a scan rate at 50 mV s^{-1}. Adapted with permission from ref. 38 and 55. Copyright 2014 American Chemical Society.

Table 1 Spectroscopic properties of BOPHYs **8–17**

Compound	R^1	R^2	R^3	Solvent	λ_{abs}[a] (nm)	λ_{em}[a] (nm)	Φ_f
8	H	H	H	CH_2Cl_2	424, *442*	465, *493*	0.95[b]
9	Me	H	Me	CH_2Cl_2	444, *467*	485, *518*	0.92[b]
10	COOEt	Me	Et	CH_2Cl_2	455, *480*	504	1.00[c]
11	Me	Et	Me	CH_2Cl_2	478, *453*	497	1.00[c]
12	Br	H	H	THF	459, *439*	482	0.25[d]
13	H	Br	H	CH_2Cl_2	439, *455*	488, *515*	0.20[e]
14	Br	Br	H	CH_2Cl_2	455, *477*	505, *537*	0.61[c]
15	Br	Br	Br	CH_2Cl_2	465, *488*	513, *546*	0.69[c]
16	Cl	H	H	Toluene	464, *442*	484, *512*	0.85[f]
17	Me	I	Me	THF	475	496	0.17[d]

[a] Secondary maxima are italicised. [b] Calculated using coumarin 540 in MeOH as a standard. [c] Calculated using fluorescein in a 0.1 M NaOH solution as a standard. [d] Calculated using rhodamine 6G in air equilibrated water as a standard. [e] Calculated using complex **8** in CH_2Cl_2 as a standard. [f] Calculated using coumarin 153 in EtOH as a standard.

to the bands observed in solution. Complex **8** shows fluorescence as a solid powder at λ_{em} = 543 nm (Φ_f = 0.12), whereas complex **9** displays fluorescence at λ_{em} = 550 nm (Φ_f = 0.28). Cyclic voltammetry (CV) was also used to probe the electronic structure of these compounds (Fig. 3d). The results show an irreversible reduction wave for **8** and **9,** with cathodic peak potentials (E_{pc}) at −1.14 and −1.03 V, respectively. On the other hand, an irreversible oxidation wave with an anodic peak potential (E_{pa}) at 1.40 V was measured for **8**, whereas **9** has a reversible oxidation wave with an E_{pa} at 1.51 V and a peak potential ($E_{1/2}$) at 1.46 V (*vs.* saturated calomel electrode (SCE)).[39]

Since the discovery of the initial BOPHYs **8** and **9**, analogous systems have been synthesized and the comparison between these systems has resulted in useful insights into important structure–property relationships. The BOPHY core functionalized with ester, methyl and ethyl groups at the α-position(s) (**10–12**) have Φ_f values nearing unity in CH_2Cl_2 – these are the highest values observed for BOPHY dyes.[38] Substitution in the α- and β-position(s) with either a methyl, ethyl, or an ester group results in a bathochromic shift of λ_{abs} and λ_{em} in comparison to the parent BOPHY (**8**). In general, brominated derivatives (**12–15**) uniformly display reduced Φ_f values. Bromination at the β-position[61] (**13**) provides a Φ_f of 0.20, however this value increases slightly to 0.25 when the BOPHY motif is brominated at the α-position (**12**).[62] Further substitution with additional bromine groups to the BOPHY scaffold (**14** and **15**)[61] increases the Φ_f value to 0.61 and 0.69, respectively (Table 1). This data shows that the degree of bromine groups appended to the BOPHY core, affects the Φ_f value (*i.e.*, the more bromine groups, the higher the Φ_f). A chlorine substituent at the α-position[63] (**16**) results in a high Φ_f of 0.85 (the highest value for a BOPHY dye substituted with a halogen), on the other hand this value drops dramatically to 0.17 upon functionalization with an iodine at the β-position[62] (**17**). The low Φ_f values of **13** and **17**, which are both mono-halogenated at the β-position, suggests that such functionalization should be avoided if high Φ_f are desired. Complex **8**, which is unsubstituted, displays the lowest λ_{max} value of all the dyes in the series (Table 1), whereas complex **11** displays the greatest bathochromic shift (54 nm) relative to the parent system **8**. The λ_{em} of **15** is 513 nm, which is the largest red-shift (48 nm) relative to complex **8**.

3. Synthesis and spectroscopic properties of BOPHYs with extended π-systems

The π-conjugation in the BOPHY dyes can be easily extended through the use of commercially available and synthetically accessible substituted pyrroles, or cross-coupling reactions starting from halogenated derivatives. These structural manipulations in turn, enable the fine-tuning of the photophysical properties of this family of dyes. For example, fusing a phenyl ring to both β-positions gives access to BOPHY derivatives that absorb in the far-red region. In this section we discuss the synthesis and spectroscopic properties of BOPYs whose π-systems are extended through derivatization of the α- and β-position(s).

One of the earliest structural modifications of the BOPHY core was reported by Son and coworkers[64] who described the synthesis (Scheme 2) and spectroscopic characterization of the alkyne derivatives **19–24**. The synthetic procedure starts with the iodination of precursor **9** (Scheme 1) at the β-position(s) (**17** and **18**) using either *N*-iodosuccinimide or a mixture of iodine

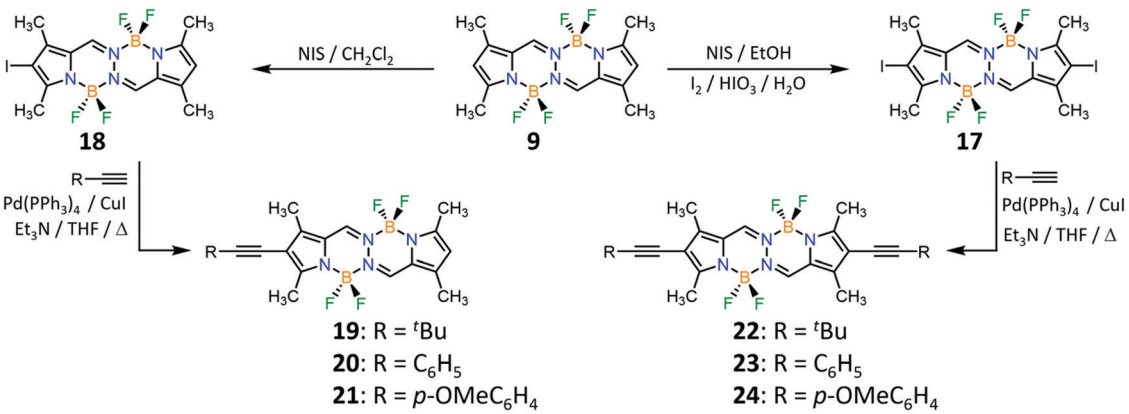

Scheme 2 Partial synthetic route towards the linearly extended BOPHY chromophores (**19–24**).

Table 2 Spectroscopic properties of BOPHY complexes **19–24**

Compound	λ_{abs}[ab] (nm)	λ_{em}[ab] (nm) solution	λ_{em}[a] (nm) solid	λ_{em}[a] (nm) film	Φ_f[c]
19	453, *475*	499, *530*	554	507, *536*	0.83
20	456, *457*	509, *536*	564	520, *544*	0.70
21	459, *479*	*523*	572	*540*	0.35
22	464, *468*	512, *544*	561	520, *542–550*	0.73
23	470, *489*	*524*	591	*536*	0.72
24	468–495	536	599	547	0.46

[a] Secondary maxima are italicised. [b] Spectra are recorded in 1,4-dioxane. [c] Calculated using quinine sulfate in a H_2SO_4 solution as a standard.

and iodic acid. The selectivity of the mono- or di-iodination was found to be strongly dependent on the number of equivalents of the halogenation reagent(s) used relative to complex **9**. Treatment with only one equivalent of the halogenation reagent results in **18** as the major product in modest yield (40%), with a minimal amount of **17** produced. Adding two equivalents of the halogenation reagent results in complex **17** in a high yield (85%). After iodination, a Sonogashira coupling reaction was used to attach the alkyne group producing complexes **19–24**, in moderate (50%) to high (79%) yields. Brominated derivatives can also be used in the same reaction sequence to yield the target complexes.

The introduction of the functionalized alkyne group(s) to the BOPHY core (**19–24**) red-shifts the main absorption band (Table 2) of the dye in comparison to complex **9** (Table 1), with the largest red shift occurring in dyes **20** and **24** which possess phenyl group terminated alkynes. The same trend is observed for the emission bands. Dyes **9** and **19–24** are emissive in the solid state as well, with the emission maxima being bathochromically shifted in comparison to the solution state. The Φ_f values of **9** and **19–24** vary from 0.35 to 0.83, with complexes **21** and **24** having the lowest values in the series. This observation is attributed to intramolecular charge transfer (ICT) from the anisole–ethynyl fragment to the BOPHY core, but additional photo-induced electron transfers and faster internal conversions from the excited state to the ground state (*i.e.*, conformation changes) cannot be discounted.[64] Density functional theory (DFT) studies were used to study this effect. The lower Φ_f values of complexes **21** and **24** were ascribed to a large difference observed in the highest occupied molecular orbital (HOMO) and the lowest unoccupied molecular (LUMO) electronic distributions. This large difference allows the ICT process to be more effective for excitation and emission, leading to the lower Φ_f values.

In 2016, Jiao and co-workers designed α-benzo-fused and β-thiophene-fused BOPHY derivatives **25–29** (Fig. 4).[65] Chromophores **25–27** were synthesized with overall yields ranging from 34 to 38% following the procedure shown in Scheme 1 starting from appropriately functionalized pyrroles. Complexes **28** and **29** were also synthesized (yields of 34 and 30%, respectively) following Scheme 1 also starting with an appropriately derivatized thienopyrrole.

The λ_{max} of the α-benzo-fused BOPHYs **25–27** are at 567, 571 and 563 nm in CH_2Cl_2, respectively. The β-thiophene-fused BOPHYs **28** and **29**, are red-shifted to λ_{max} = 591 and 600 nm in CH_2Cl_2, respectively as a consequence of the extended π-delocalization (Fig. 5a). In comparison to the parent BOPHY (**8**), the λ_{max} of **26** is bathochromically shifted by over 140 nm, whereas **28** has a bathochromic shift of over 175 nm. Red-shifted fluorescence bands in CH_2Cl_2 are also observed for all the dyes with λ_{em} ranging from 602 to 648 nm (Fig. 5b). Increasing the solvent polarity from toluene to acetonitrile induces a minor blue-shift in the absorption and emission bands (*e.g.*, λ_{em} for **25** in toluene is 611 nm and 601 nm in acetonitrile), though no explanation is given for this effect.

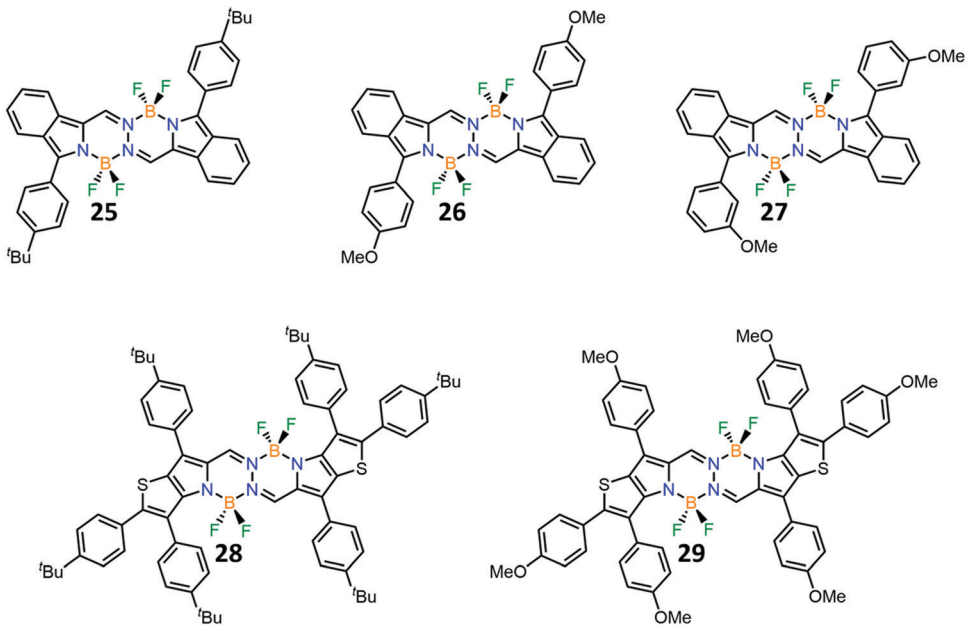

Fig. 4 Chemical structures of α-benzo-fused (**25–27**) and β-thiophene-fused (**28** and **29**) BOPHY derivatives.

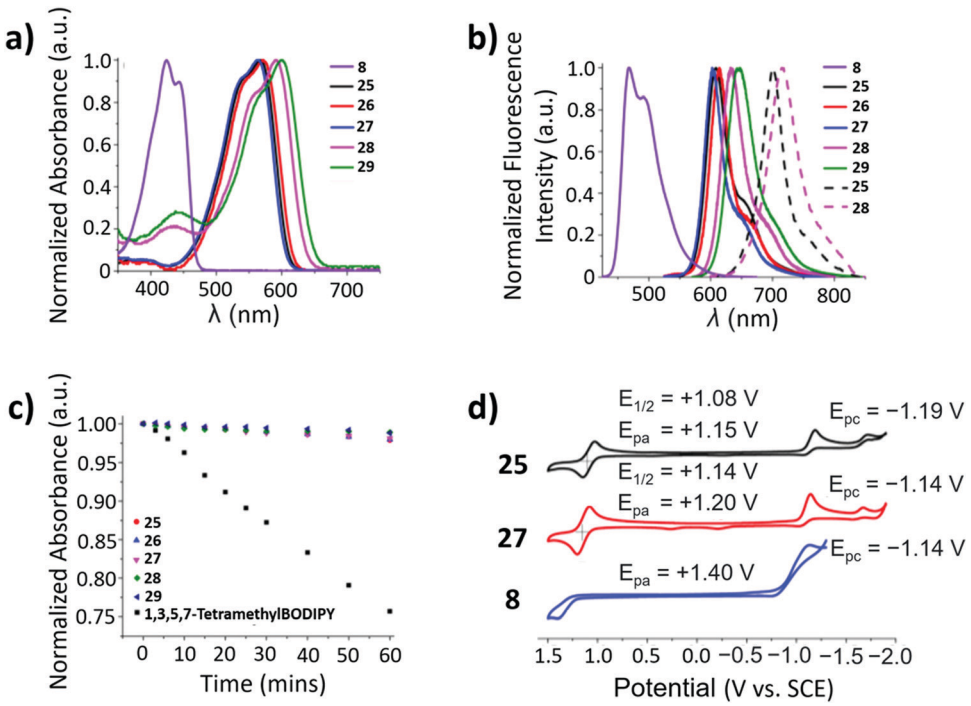

Fig. 5 (a) Normalized absorption and (b) fluorescence emission spectra of BOPHY complexes **8** and **25–29** in CH_2Cl_2 (solid lines) and in the solid state (dashed lines). (c) Photostability comparison of BOPHYs **25–29** against 1,3,5,7-tetramethyl BODIPY in air-saturated toluene by absorbance monitoring during continuous irradiation with a 500 W Xe lamp over 60 minutes (35 mW cm^{-2}; 25 °C). (d) CVs of **8**, **25** and **27** (1 mM) measured in CH_2Cl_2 at 25 °C containing $TBAPF_6$ (0.1 M) as the supporting electrolyte, glassy carbon as the working electrode with a scan rate at 50 mV s^{-1}. Adapted with permission from ref. 66. Copyright 2016 American Chemical Society.

The Φ_f values of **25–29** in various solvents range from 0.22 to 0.64, decreasing slightly when the solvent is changed from toluene to acetonitrile. In CH_2Cl_2, the β-thiophene-fused BOPHYs **28** (λ_{em} = 631 nm, Φ_f = 0.60) and **29** (λ_{em} = 648 nm, Φ_f = 0.50) emit strongly in the red region. α-Benzo fused BOPHYs (**25–27**) show weaker emission in the red region with Φ_f values ranging from 0.31 to 0.36. The Φ_f values of all these complexes are all lower when compared against the parent BOPHY system **8**. Powders of α-Benzo-fused BOPHY **25** and β-thiophene-fused **28** show near-infrared (NIR) fluorescence centered at 701 nm (Φ_f = 0.10) and 717 nm (Φ_f = 0.13), respectively (Fig. 5b). BOPHY dyes **25–29** also exhibit high photostabilities (Fig. 5c). Following irradiation over 60 minutes, the absorbance of dyes **25–29** diminish slightly in comparison to the well-known commercial dye 1,3,5,7-tetramethyl BODIPY (4,4-difluoro-1,3,5,7-tetramethyl-4-bora-3*a*,4*a*-diaza-*s*-indocene) whose absorption diminishes to 76% of its original value under the same conditions. DFT calculations were employed to estimate the HOMO and LUMO energy levels and notably, the fusion of benzo rings at the BOPHY core was found to cause a large increase in the HOMO energy level. In comparison with **8**, these results indicate that benzene-fused structures mainly increase the HOMO energy level, thus decreasing the energy band gap.[66]

Liu and Han synthesized the furan analogues (**30–32**)[67] as shown in Scheme 3. The starting material **33** was synthesized using a Suzuki–Miyaura cross-coupling reaction between commercially available reagents 5-bromofuran-2-carbaldehyde and 4-anisylboronic acid. A Hemetsberge–Knittel reaction was then employed to form **34**, followed by regioselective bromination to give either **35**, **36** or **37** in high yields (>80%). A Suzuki–Miyaura cross-coupling reaction between the corresponding bromine derivatives and 4-anisylboronic acid affords compounds **38–40**. A decarboxylation reaction under basic conditions afforded compounds **41–43**, which were subjugated to Vilsmeier–Hack reaction conditions to form the key precursors **44–46** in yields above 80%. These compounds were then used to form the targeted BOPHY complexes in yields ranging from 45 to 52%.

Dyes **30**, **31** and **32** exhibit a λ_{max} at 606, 622 and 624 nm, respectively, in CH_2Cl_2. These values are marginally red-shifted in comparison to the α-benzo- or β-thiophene-fused complexes **25–29**. The ε values range are 109 700, 121 300 and 123 000 M^{-1} cm^{-1} for **30**, **31** and **32**, respectively. The emission bands for BOPHYs **30**, **31** and **32** (Fig. 6b) are also generally red-shifted in comparison to **25–29** with λ_{em} of 646, 661 and 667 nm, respectively. The absorption and emission maxima display minor solvent dependency, and the dyes show high photostabilities in the solution state. The Φ_f value of the dyes in CH_2Cl_2 range from 0.34 to 0.40 with BOPHYs **30** and **32** displaying the highest and lowest values, respectively. DFT calculations (Fig. 6c) show that the HOMO and LUMO levels of dyes **30–32** have similar electronic distributions and that substitution at the α-position of the furan ring with a 4-*n*-butoxyphenyl group can induce ICT from the phenyl ring to the BOPHY core, resulting in the modest Φ_f values.[67]

In 2015, Ziegler and Nemykin synthesized a diferrocene-functionalized BOPHY complex, which displayed a broad absorption band with λ_{max} at 700 nm. This band was attributed

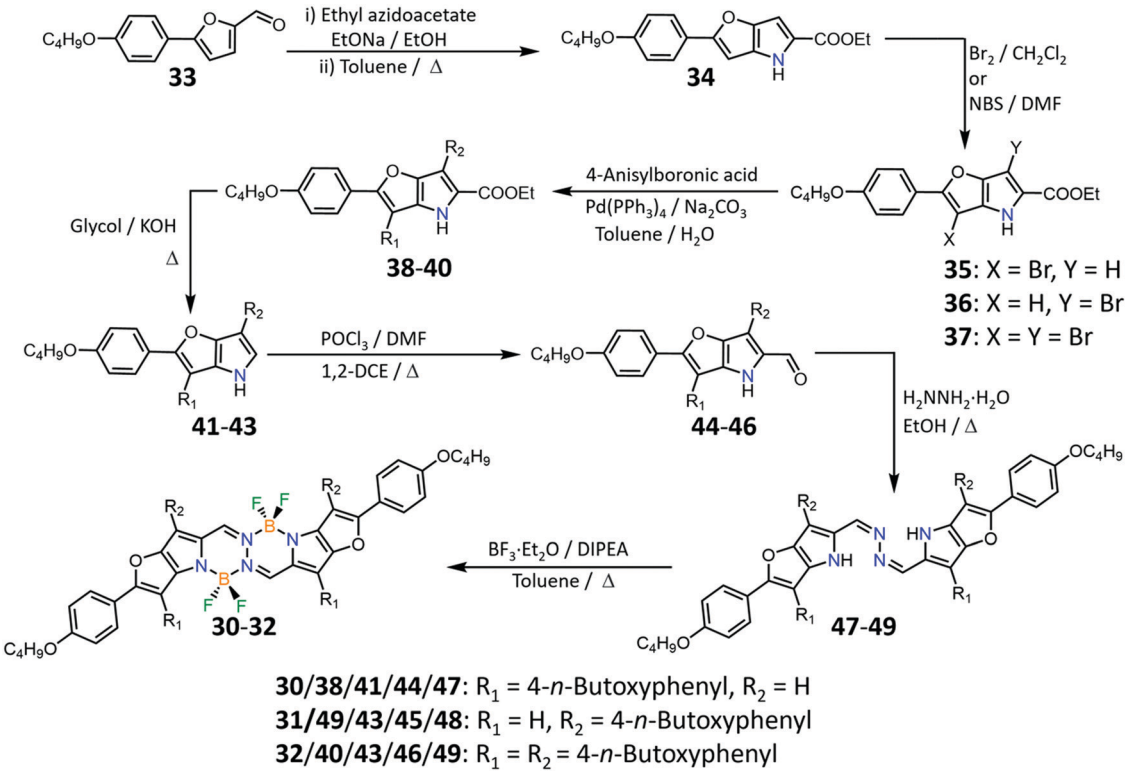

Scheme 3 Synthetic route towards the furan-fused BOPHY chromophores **30–32**.

to metal-to-ligand charge-transfer as well as core-centered π–π* transitions with TD-DFT studies confirming this hypothesis.[68] Harriman and co-workers have also identified and quantified unexpected long-range electrostatic interactions in a BOPHY compound functionalized with two amine groups following protonation or oxidation.[69] Subsequently, Ziegler and Nemykin studied the effect of electron-withdrawing ester groups affixed to the β-pyrrolic position of the ferrocene-functionalized dyes **50** and **51**.[70] The complexes were synthesized (Fig. 7a) starting from an appropriately functionalized pyrrole, which was subjugated to Vilsmeier–Hack reaction conditions to install an aldehyde functional group. The obtained pyrrole was then reacted as shown in Scheme 1 to form the complex **52**. A Knoevenagel condensation of **52** with ferrocene carboxaldehyde affords the BOPHY dyes **50** and **51** in low yields of 12 and 21%, respectively.

The structure of complex **50** was elucidated by X-ray crystallography (Fig. 7b), revealing an inversion center. The atoms within the core of BOPHY **50** are coplanar with the vinyl ferrocene substituents and one of the cyclopentadienyl rings residing within the same plane. Both the phenyl and ester functional groups are twisted in a perpendicular manner with respect to the BOPHY core, suggesting a break in the π-conjugation at these positions.[70] The structure of BOPHY **50** is consistent with the solid-state structures of the first BOPHY systems **8** and **9**, where only the fluorine atoms deviate from the plane.[55,56] The absorption spectra (Fig. 7c) of BOPHY complexes **50** and **51** are similar to the first ferrocene-containing BOPHY[68] synthesized by Ziegler and Nemykin as well as ferrocene-functionalized BODIPYS.[71] The absorption spectra show a narrow band with λ_{max} = 497 and 514 nm and a broader band at λ_{max} = 606 and 656 nm for **50** and **51**, respectively. Fluorescence in **50** and **51** is quenched, confirming the presence of an electron-transfer pathway from the ferrocene-centered molecular orbitals to the photo-excited states of both compounds.

Inspired by dihalogenated BODIPY derivatives undergoing S_NAr reactions[72–76] with a wide range of nucleophiles, Hao and coworkers used dibrominated BOPHY (**14**) to synthesize dyes **53–55** (Fig. 8a).[61] Reacting **14** with either three or six equivalents of *n*-butylamine in dichloroethane results in either the monosubstituted BOPHY **53** or the disubstituted BOPHY **54**, respectively, in high yields (>80%). Dye **55** was obtained in a 78% yield by first reacting with the less reactive nucleophile 4-*tert*-butylaniline followed by a subsequent reaction with diethylamine. The structure of BOPHY **55** was confirmed by X-ray crystallography, revealing a highly twisted conformation of the BOPHY core. The two amino-substituted groups in BOPHY **55** generate sufficient steric hindrance to disrupt the planarity of the BOPHY core.

The absorption and emission bands of **53–55** in CH_2Cl_2 are red-shifted in comparison to BOPHY **14** (λ_{max} = 455 nm, λ_{em} = 505 nm, Φ_f = 0.61, and ε = 20 000 M^{-1} cm^{-1}). The λ_{max} of **53** is at 497 nm with an λ_{em} at 558 nm. The λ_{max} and λ_{em} of **54** with its two butyl-bearing amines are red-shifted to 540 and 565 nm, respectively. Dye **55** with its two different amines exhibits the most red-shifted absorption and emission bands (λ_{max} = 545 nm and λ_{em} = 590 nm), most likely because of the presence of the *tert*-butylaniline group. As for the emission efficiency, **53** exhibits extremely weak

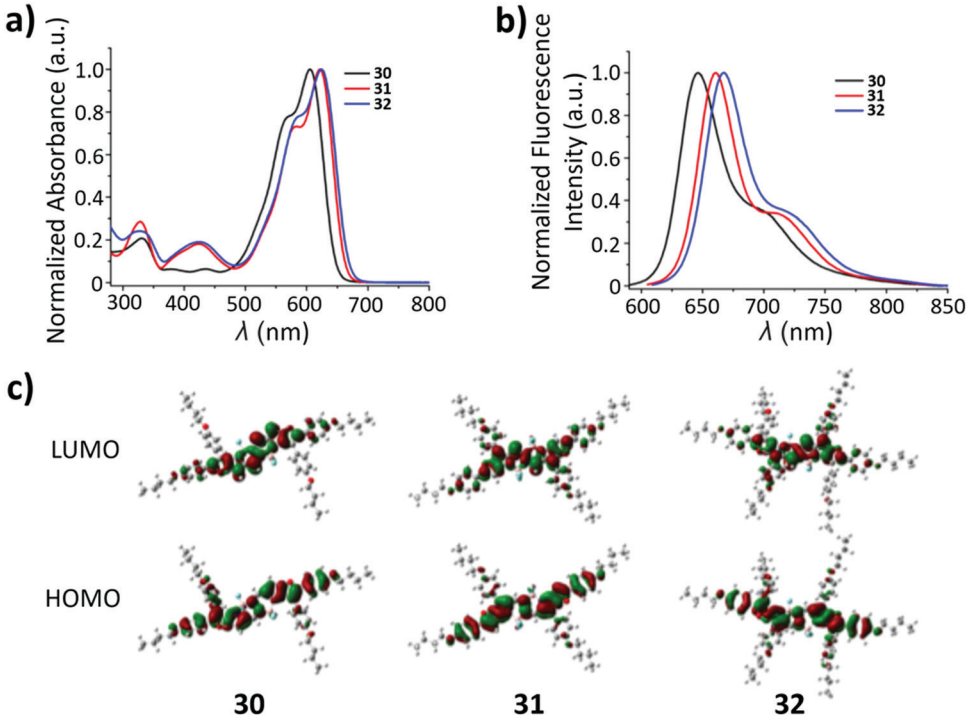

Fig. 6 (a) Normalized absorption and (b) fluorescence spectra of BOPHY complexes **30–32** in CH_2Cl_2. (c) Electron density distributions in the HOMO and LUMO states calculated by DFT. Adapted with permission from ref. 68. Copyright 2016 American Chemical Society.

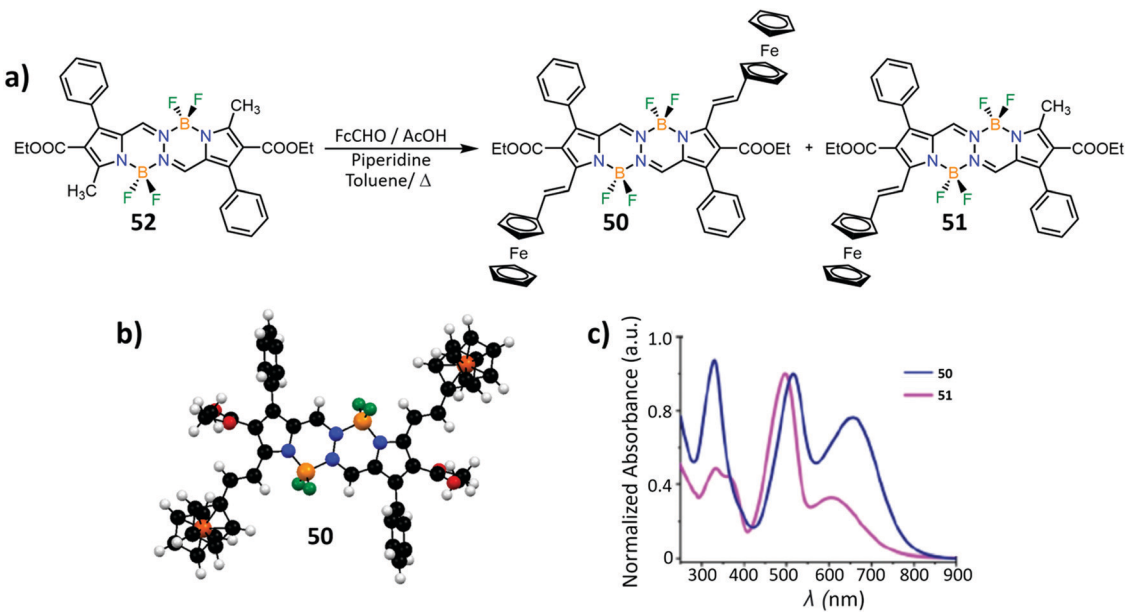

Fig. 7 (a) Partial synthesis of ferrocene containing BOPHYs **50** and **51**. (b) X-Ray structure of BOPHY complex **50** shown in ball and stick representation. Fluorine, boron, nitrogen, oxygen, iron, carbon, and hydrogen atoms are indicated by green, light orange, blue, red, dark orange, black, and white respectively. (c) Normalized absorption spectra of BOPHY complexes **50** and **51** in CH_2Cl_2. Adapted from ref. 71. Copyright Wiley-VCH GmbH. Reproduced with permission.

fluorescence with a Φ_f of 0.01, while **54** and **55**, display comparatively bright red fluorescence with slightly better Φ_f values of 0.33 and 0.14, respectively. The ε values of **53**, **54** and **55** (45 700, 50 100 and 56 200 M^{-1} cm^{-1}, respectively) increase when going from one to two amine substituents and finally diethylamine and a 4-*tert*-butylaniline group.

Hao and co-workers[61] also synthesized dye **56** (Scheme 4a) in a low yield of 37% by heating BOPHY **15** in toluene in the presence

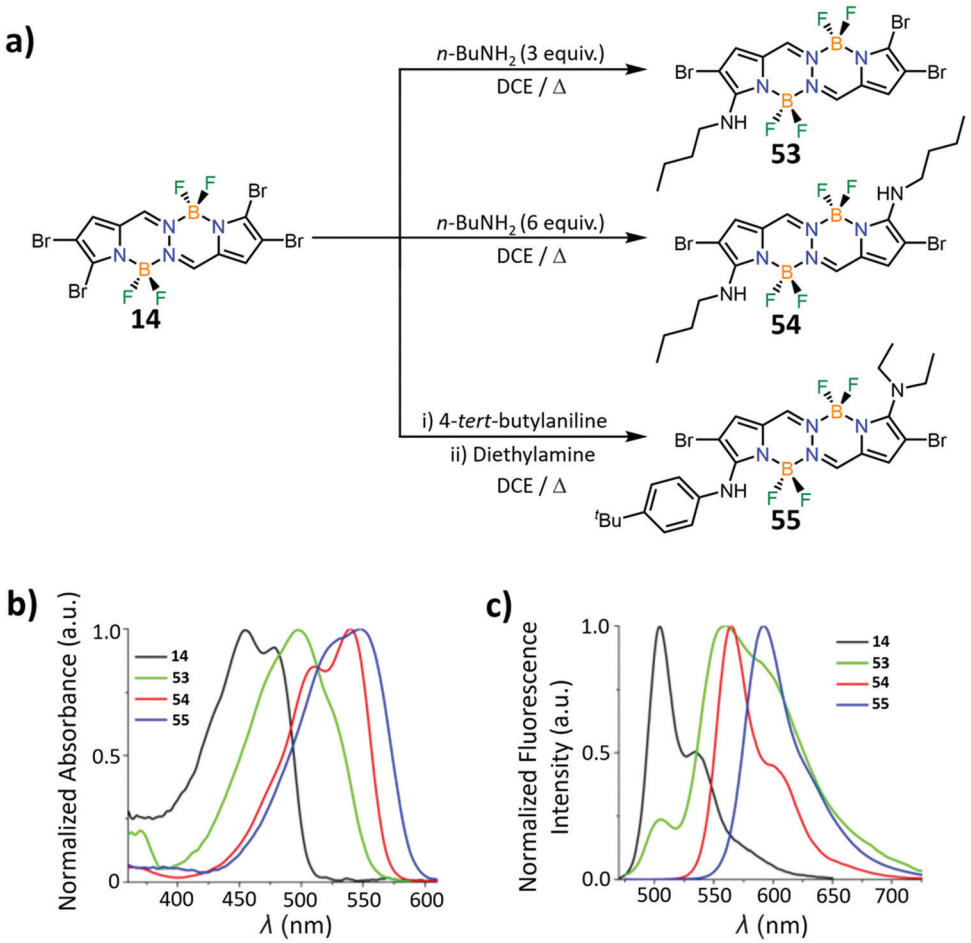

Fig. 8 (a) Partial synthetic route from brominated BOPHY **14** to BOPHYs **53–55**. (b) Normalized absorption and (c) fluorescence emission spectra of BOPHY **14** and BOPHYs **53–55** in CH_2Cl_2. Adapted with permission from ref. 61. Copyright 2018 American Chemical Society.

of 114 equivalents of pyrrole. Despite the significant excess of reagent, only the monopyrrole-substituted complex was observed. Next, they used Suzuki and Stille coupling reactions to form BOPHYs **57** and **58** in high yields of 83 and 86%, respectively (Scheme 4b). The structures of both **57** and **58** were confirmed by X-ray structure analysis, which showed that the aryl and thiophene rings at the 5,5′-positions are coplanar with the BOPHY core. The dihedral angles between the BOPHY core and either the phenyl or thiophene ring were observed to be less than 9°.

The λ_{max} and λ_{em} of the monopyrrole-substituted BOPHY (**56**) in CH_2Cl_2 are 557 and 630 nm, respectively. Although the absorption and emission maxima are significantly red-shifted in comparison to the parent BOPHY **8**, the Φ_f value is substantially lower at 0.05, indicating that simple structural changes can drastically alter the photophysical properties of the dye. The ε value of BOPY **56** is 46 800 M^{-1} cm^{-1}, marginally higher than that of BOPHY **8**. Installing electron-donating substituents at the *para*-position of the phenyl rings (**57**) results in a bathochromic shift of 150 and 189 nm in λ_{max} and λ_{em} in CH_2Cl_2, respectively, when compared against BOPHY **8** (Fig. 9a and b). Similarly, thiophene-substituted BOPHY **58** also exhibit red-shifted absorption and emission bands (λ_{max} = 516 nm, and λ_{em} = 572 nm) compared to **8**. Both **56** and **57** show a gradual decrease of Φ_f value with increase in solvent polarity. For example, fluorophore **57** has a Φ_f of 0.39 in hexanes, which decreases to 0.12 in toluene and further to 0.09 and 0.04 in CH_2Cl_2 and tetrahydrofuran, respectively. No explanation is given for this observation.

The authors also took advantage of the pH sensitivity of **57** to study the effect of protonation on the photophysical properties of the dye. A solution of **57** in toluene was titrated with trifluoroacetic acid (TFA) and the spectra showed a stepwise disappearance of the absorption band at λ_{max} = 590 nm with the simultaneous appearance of a new band at λ_{max} = 495 nm (Fig. 9c). Similarly, a blue-shift of the emission band (Fig. 9d) was observed from λ_{em} = 634 to 530 nm with an eight-fold increase in fluorescence intensity because of the inhibition of the ICT process from the diethylamine moiety to the BOPHY core. In a mixture of acetonitrile and water, similar results were observed with fluorescence intensity increasing as conditions became more acidic.

More recently, Shen and co-workers synthesized BOPHYs possessing phenyl (**59**) or thiophene (**60**) functional groups attached to the β-positions and investigated their photophysical properties.[77] The complexes were synthesized by Stille cross-coupling reactions using intermediate **17** (Fig. 10a) to give dyes

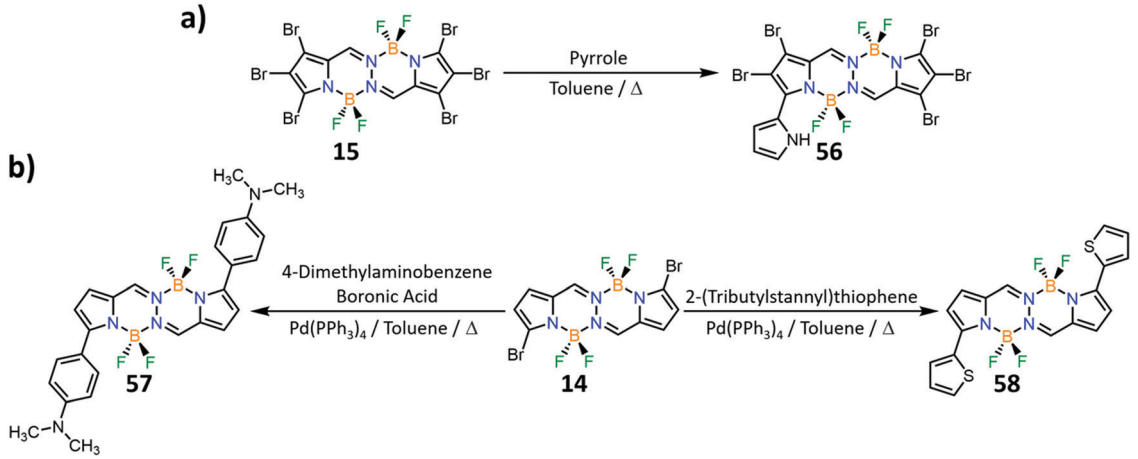

Scheme 4 Partial synthetic route towards aryl substituted BOPHYs **56–58** from brominated BOPHYs **14** and **15**.

59 and **60** in yields of 52 and 61% respectively. X-Ray crystallography analysis showed that in complex **59** the dihedral angle between the phenyl ring and the BOPHY core is 41.6°, significantly larger to that of complex **60**, where the angle is 27.3°. This observation suggested that the π-conjugation in **60** should be better as it is more planar, resulting in a red-shift compared to the parent BOPHY system. Differences in the packing arrangements were also observed (Fig. 10b). Dye **59** shows face-to-face intermolecular stacking in parallel planes, whereas **60** displays slipped stacking. Moreover, a slip angle of ~90° was observed in **59** (attributed to H-aggregation), whereas a slip angle of 46° was observed for **60** indicating J-aggregation.[78] These observations suggest that the introduction of a substituent at the β-position has a significant impact on the molecular packing.

The introduction of the thiophene group at the β-positions (**60**) induces a red-shift in λ_{max} and λ_{em} relative to dye **59**; however, both dyes show strong solvent dependency as fluorescence quenching is observed with an increase in solvent polarity (Table 3). For example, **60** emits at λ_{em} = 522 nm with a Φ_f value of 0.74 in hexanes and is red-shifted to 558 nm with a reduced Φ_f value of 0.02 in acetonitrile. These changes, observed with an increase in solvent polarity, are attributed to excited-state conformational states which drive faster internal

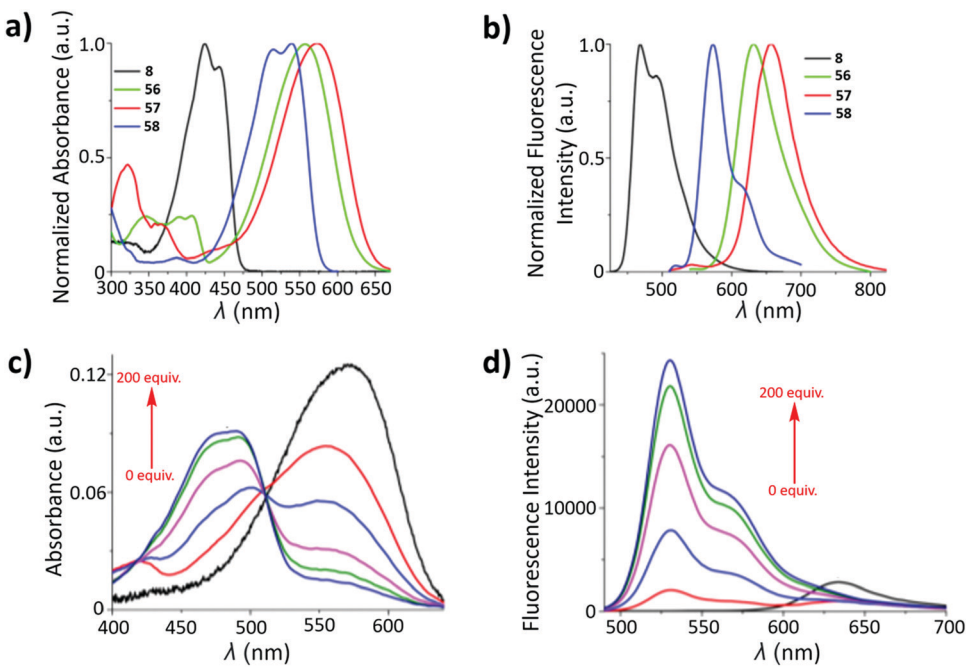

Fig. 9 (a) Normalized absorption and (b) fluorescence emission spectra of BOPHY **8** and BOPHYs **56–58** in CH_2Cl_2. (c) Absorption and (d) fluorescence spectra of fluorophore **57** (4.5 μM in toluene) with incremental addition of TFA when excited at 470 nm. Adapted with permission from ref. 61. Copyright 2018 American Chemical Society.

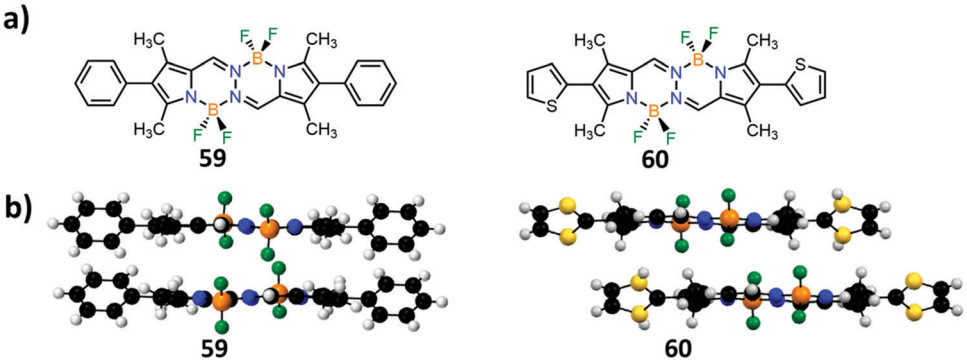

Fig. 10 (a) Structural formulas of BOPHYs **59** and **60**. (b) Crystal packing of BOPHY complexes **59** and **60** shown in ball and stick representation. Fluorine, boron, nitrogen, sulfur, carbon, and hydrogen atoms are indicated by green, light orange, blue, yellow, black, and white respectively.

Table 3 Spectroscopic properties of BOPHY complexes **59** and **60**

Compound	Solvent	λ_{abs}[a] (nm)	λ_{em}[a] (nm)	ε (M^{-1} cm^{-1})	Φ_f
59	Hexanes	482, *457*	506	110 470	0.88
	THF	480, *457*	507	101 340	0.84
	CH_3OH	475, *453*	502	98 540	0.86
	CH_3CN	453, *472*	503	97 010	0.86
60	Hexanes	485	522	95 250	0.74
	THF	481	537	119 060	0.15
	CH_3OH	475	540	114 200	0.10
	CH_3CN	473	558	116 610	0.02

[a] Secondary maxima are italicised.

conversion to the ground state, in turn quenching the emission.[79,80] This trend is reflected by an increase in the non-radiative decay rate, changing from 0.96×10^8 s^{-1} in hexanes to 65.33×10^8 s^{-1} in acetonitrile. In the solid state the Φ_f of **59** and **60** are 0.10 and 0.11, respectively. As J-aggregates are observed in the crystal packing of **60**, the authors expected a higher Φ_f. However, in BODIPY systems the addition of a thiophene group introduces additional intersystem crossing pathways, which can reduce Φ_f.[81] In support of this, TD-DFT studies indicate that ICT occurs from the thiophene group to the BOPHY core.

BOPHY **60** exhibits good solubility in methanol but poor solubility in water. Studies into the influence of aggregation on photophysical properties were hence conducted by varying the fraction of water (f_w by volume) in a methanol solution of **60**. The absorption spectra (Fig. 11a) show no difference up to a f_w of 20%. Subsequently, at f_w of 40%, the band at λ_{max} = 474 nm diminishes completely and a new broad absorption band forms at λ_{max} = 560 nm. At f_w of 40%, the emission band (Fig. 11b) centered at 540 nm disappears, and a new band at λ_{em} = 585 nm with a shoulder at 627 nm appears. These photophysical changes are characteristic of the presence of J-aggregates.[82] At f_w of 60%, the absorption spectrum shows three separated bands centered at 493, 528 and 586 nm, which are attributed to the formation of multiple J-aggregates having different geometries.[83,84] From f_w of 70% to 90%, the absorption bands gradually decrease. Interestingly, BOPHY **59** did not show any evidence of aggregation under the same conditions.

4. Applications of BOPHY dyes

The easily tunable photophysical properties (*e.g.*, Φ_f and λ_{max}) of BOPHY dyes in combination with their ease of synthesis, have accelerated their adaptation and use within various research fields. One of the earliest applications of the BOPHY motif was reported by Jiang and co-workers in 2015,[85] who demonstrated the pH-dependent fluorescence behavior of BOPHY **61** and its potential use as a 'switch on' pH sensor (Fig. 12a). Controlling

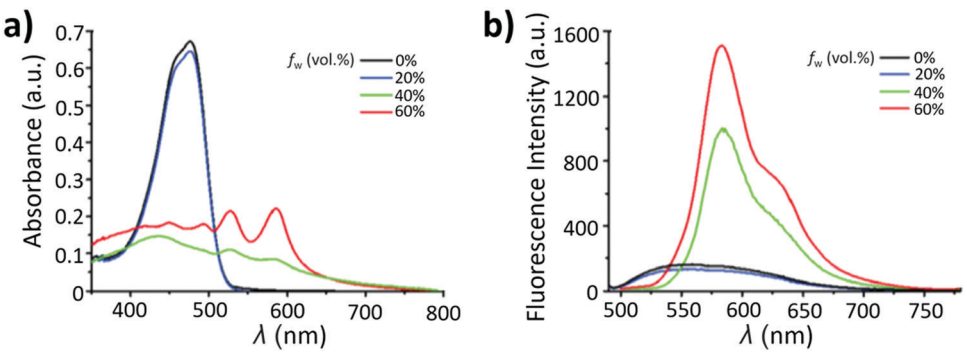

Fig. 11 (a) Variation in absorption and (b) emission spectra of **60** with incremenal addition of H_2O in MeOH. Adapted from ref. 77 with permission from The Royal Society of Chemistry.

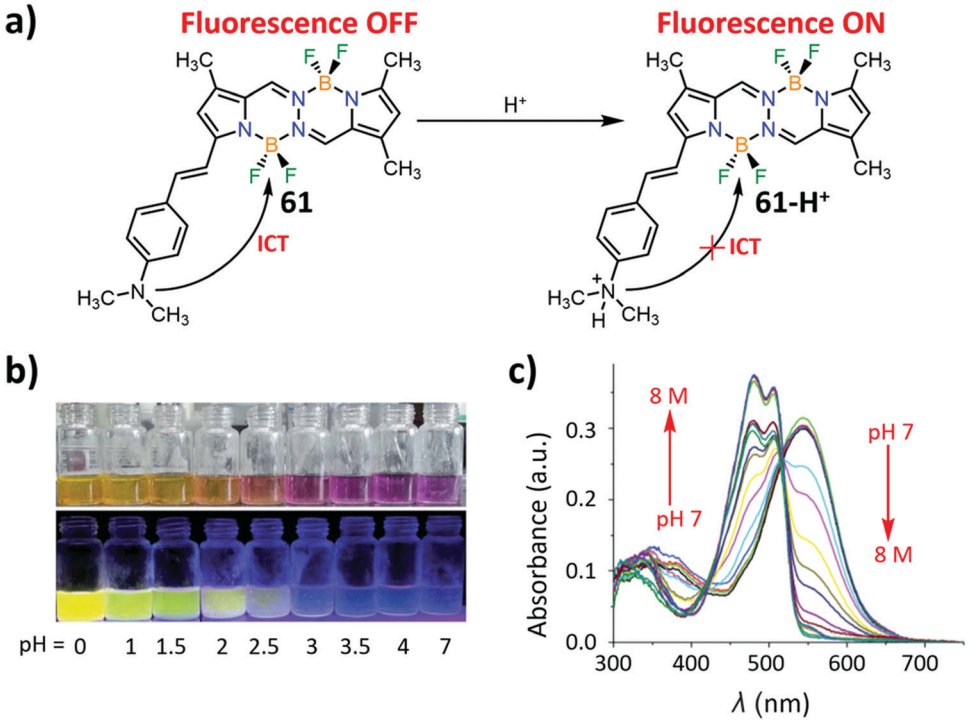

Fig. 12 (a) Protonation of BOPHY **61** inhibits quenching of the excited state by ICT, generating the fluorescent BOPHY **61-H$^+$** species. (b) Photographed solutions of BOPHY **61** (5 μM in $CH_3CN–H_2O$ (1 : 1)) with varying pH under ambient light (top) and UV irradiation (bottom). (c) Variation in absorption spectra of **61** (5 μM in $CH_3CN–H_2O$ (1 : 1)) with incremental acidification (pH 7 to 8 M HCl). Adapted from ref. 85 with permission from The Royal Society of Chemistry.

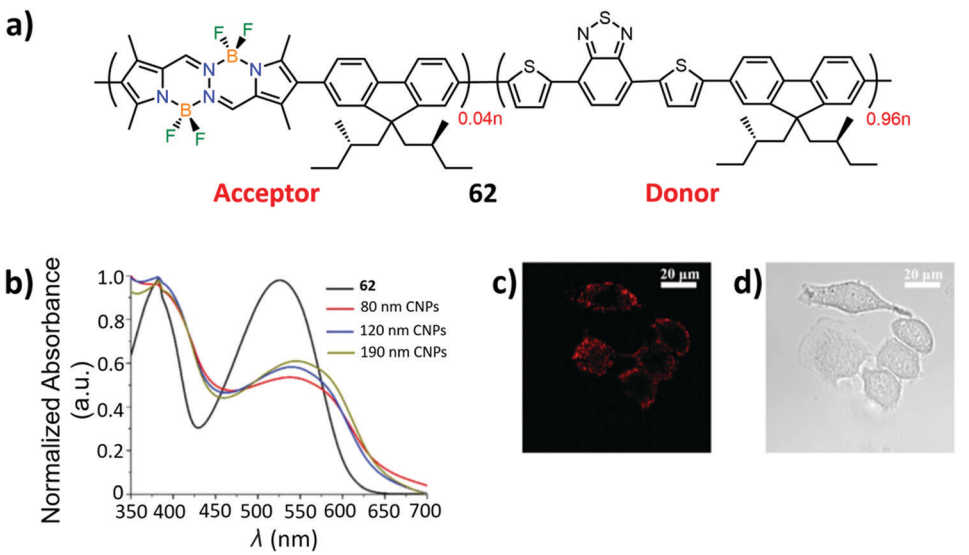

Fig. 13 (a) Chiral conjugated polymer **62** (molar ratio indicated in red). (b) Absorption spectra of **62** and CNPs with diameters of 80, 120 and 190 nm in THF (20 ppm). Confocal microscopy images of living HeLa cells at 2 hours after incubation with the 80 nm diameter CNP upon (c) excitation at 559 nm and (d) a bright field image. Adapted from ref. 88 with permission from The Royal Society of Chemistry.

ICT is a popular strategy[86,87] when designing pH-responsive fluorescent sensors, therefore Jiang and co-workers incorporated a diethylamine group for this purpose in their design of the dye. The expectation was that **61** would behave in a similar manner to BOPIHY pH probes whereby the fluorophore will be quenched through electron transfer from the electron donating group (*i.e.*, an amine).[86]

To first demonstrate that protonation 'switches off' the electron transfer, and in turn 'switches on' fluorescence emission, the researchers studied the photophysical properties of BOPHY **61** at

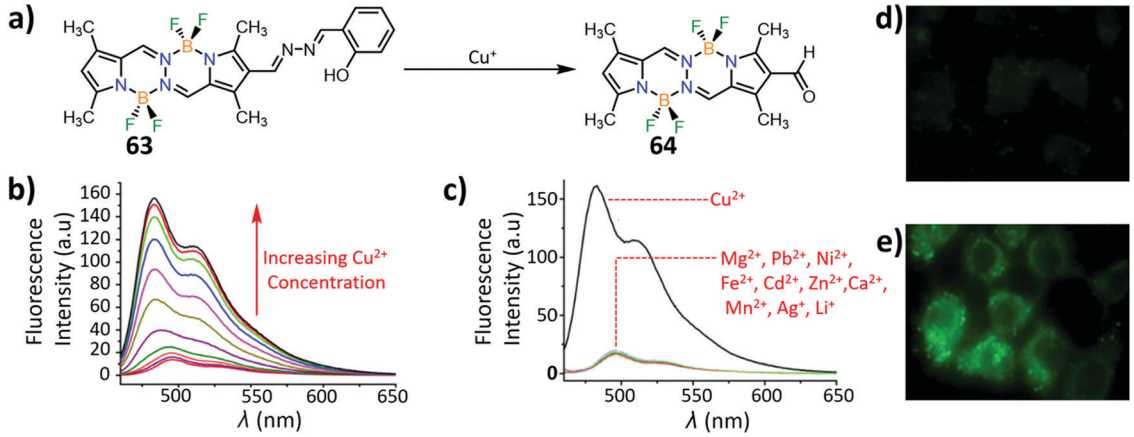

Fig. 14 (a) Addition of Cu^{2+} to **63** mediates hydrolysis, giving the fluorescent species **64**. (b) Variation in emission intensity of **63** (1 μM in CH_3CN–phosphate buffer (1 : 1) (phosphate buffer, 10 mM, pH 7.4)) with Cu^{2+} addition (increments from 0 to 40 μM). (c) Selectivity study of **63** (1 μM in CH_3CN–phosphate buffer (1 : 1) (phosphate buffer, 10 mM, pH 7.4)) in the presence of Cu^{2+} (10 μM) compared with other metal ions (100 μM) (Mg^{2+}, Pb^{2+}, Ni^{2+}, Fe^{2+}, Cd^{2+}, Zn^{2+}, Ca^{2+}, Mn^{2+}, Ag^{+} and Li^{+}). Fluorescence images of living HeLa cells under the excitation of blue light after 2 hours incubation with (d) 1 μM of **63** and (e) 1 μM of **64** with 20 μM Cu^{2+}. Adapted from ref. 90 with permission from Elsevier.

pH levels ranging from seven to zero (Fig. 12b). They observed a dramatic increase in fluorescence intensity with decreasing pH – this is attributed to protonation of the diethylamine group in **61**, inhibiting ICT. Following this observation, absorption spectra were recorded with addition of acid (up to 8 M) to a solution of BOPHY **61** (Fig. 12c). The spectra show a stepwise decrease of the absorption band at λ_{max} = 543 nm with decreasing pH. Simultaneously, the formation of two new bands at λ_{max} = 504 and 481 nm were observed, corresponding to the formation of **61-H$^+$**. The monitoring of fluorescence emission under similar conditions, revealed a dramatic increase in fluorescence intensity with the band at λ_{em} = 532 nm increasing in intensity by 1200-fold. The Φ_f of BOPHY **61** was determined to be 0.01 at pH 7 ('off') in a 1 : 1 solution of acetonitrile and water, and 0.98 ('on') when treated with a solution of hydrochloric acid (4 M). DFT calculations were employed to confirm that ICT from the diethylamine group to the BOPHY core quenches emission, while protonation inhibits ICT thus turning emission 'on'.

Chen and Wang in 2015 reported on the first use of the BOPHY motif in cell imaging.[88] The researchers synthesized the chiral polymer **62** (Fig. 13a), which was subsequently used to prepare conjugated polymer nanoparticles (CNPs) with average sizes of ~80, ~120 and ~190 nm. The absorption spectra of polymer **62** and the different sized CNPs were recorded in tetrahydrofuran (Fig. 13b). Polymer **62** exhibits two absorption bands at λ_{max} = 380 and 530 nm. The CNPs have a shoulder peak around 380 nm in addition to a band at λ_{max} = 551 nm. These bands experience a small red-shift as the particle size increases from 80 to 190 nm. The red-shift is most likely related to the formation of nanoparticle aggregates which are able to enhance inter- and intra-chain interactions.[89] Fluorophore **62** is shown to exhibit strong fluorescence at λ_{em} = 642 nm. As the size of the CNPs increase from ~80 to ~190 nm, the λ_{em} also red-shifts from 660 nm to 671 nm – this is attributed to the enhanced interaction between the polymer chains as the nanoparticles grow. The 80 nm CNP was selected for cell imaging studies in living HeLa cells because of its smaller diameter. The cells were incubated with a suspension of the 80 nm CPN for two hours at a temperature of 37 °C followed by excitation at 559 nm. Uptake of the 80 nm CNPs by the cells was clearly visualized with apparent localization at the periphery of the cytoplasm (Fig. 13c and d). This particular size of CNP was found to display high photostability and low cytotoxicity, evident by regular cell function, indicating the potential of these CNPs as efficient far-red/NIR fluorescent probes.

In 2016 Yu and co-workers[90] designed probe **63** and used it in the detection of Cu^{2+} ions (Fig. 14a). BOPHY **63** was found to fluoresce weakly – this was attributed to the deactivation of the

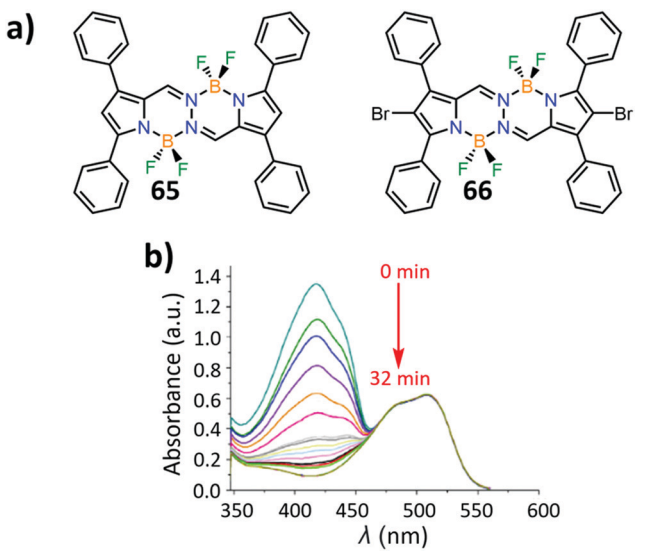

Fig. 15 (a) BOPHY **65** and its brominated analogue **66**. (b) Time-dependent decrease (increments from 0 to 32 minutes) of DPFB absorbance at 416 nm (5 μM in toluene) in the presence of **66** (6 μM in toluene), and absorption spectra of **66** (bottom curve) (5 μM in toluene). Monochromatic light (500 nm at 0.5 mW cm^{-2}) was used in the irradiation experiment. Adapted from ref. 99 with permission from Elsevier.

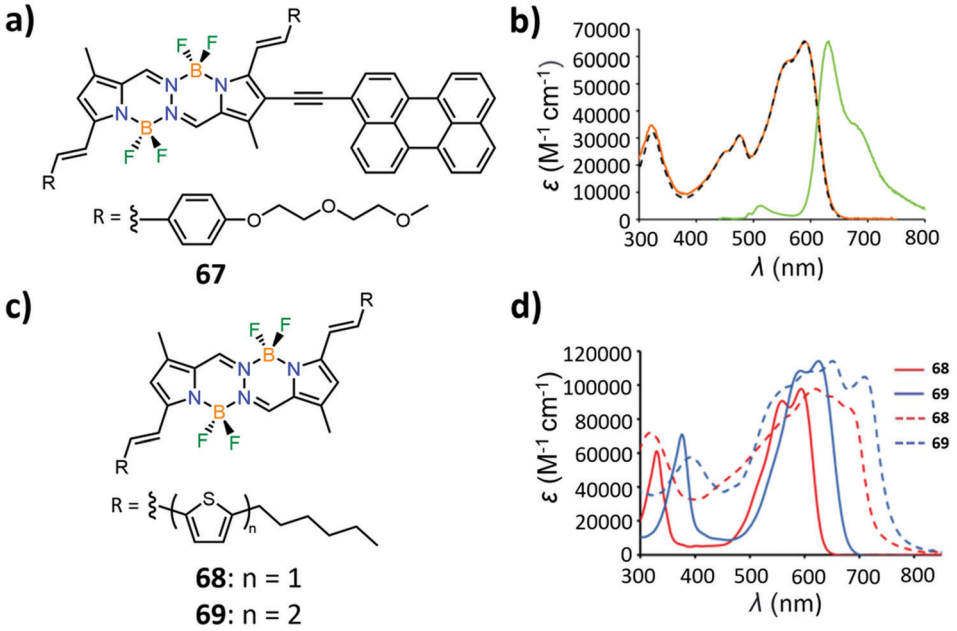

Fig. 16 (a) Chemical structure of BOPHY **67**. Absorption (orange), excitation (dashed black, λ_{em} = 631 nm) and (b) emission (green, λ_{exc} = 590 nm) spectra of **67** in THF. (c) Chemical structures of BOPHYs **68** and **69**. (d) Absorption spectra of **68** (solid red) and **69** (solid blue) in THF, as well as thin films of **68** (dashed red) and **69** (dashed blue) The absorption of the films (optical density of about 0.5) is normalized to the absorption in solution. Adapted with permission from ref. 62. Copyright 2015 American Chemical Society. Adapted from ref. 105 with permission from The Royal Society of Chemistry.

excited state *via* non-radiative pathways associated with the rapid isomerization of the C=N double bond.[91–93] Upon addition of Cu^{2+} (20 μM), a significant enhancement of fluorescence was observed as a result of the Cu^{2+} mediated hydrolysis of the C=N group yielding the emissive fluorophore **64**.

Sensitivity studies show that the fluorescence intensity progressively increased as a function of Cu^{2+} concentration (from 0 to 40 μM) (Fig. 14b). The detection limit was assessed to be 50 nM, comparable to other reported Cu^{2+} assay methods.[94,95] Further studies revealed high selectivity of the hydrolysis process towards Cu^{2+} and negligible fluorescence change was observed with a range of other cationic metal species (Fig. 14c). Competition experiments examining emission intensity of **63** (1 μM) in the presence of 10 μM of Cu^{2+}, in addition to a significant excess (100 μM) of other metal ions (Mg^{2+}, Pb^{2+}, Ni^{2+}, Fe^{2+}, Cd^{2+}, Zn^{2+}, Ca^{2+}, Mn^{2+}, Ag^{+} and Li^{+}), show clear specificity for Cu^{2+} with a lack of interference from other ions. Cu^{2+} sensing was also performed in diluted human serum samples and living HeLa cells. The results show that the amount of Cu^{2+} detected was within the required range for human serum[96] and that HeLa cells containing 1 μM of **63** alone showed, as expected, weak green fluorescence (Fig. 14d). However, when 1 μM of complex **63** is incubated with 20 μM of Cu^{2+}, strong green fluorescence is observed (Fig. 14e). These results demonstrate that **63** can be used in sensing Cu^{2+} within biological environments. Additional work from Yu and coworkers resulted in further improvement on the probe including a 50-fold increase in sensitivity (*i.e.*, down to 1 nM detection limit).[97] A similar mechanism was also later on used in the sensing of Cd^{2+} ions.[98]

Jiang and coworkers further developed the BOPHY motif as a photosensitizer for singlet oxygen generation (Fig. 15).[99] Using reported literature procedures,[54,100] precursor **65** was brominated, generating fluorophore **66** in a yield of 64%. The λ_{max} of **66** is at 506 nm, which is largely offset from the λ_{max} of the singlet oxygen scavenger 1,3-diphenylisobenzofuran (DPFB; 416 nm) making it a suitable photosensitizer. To probe the

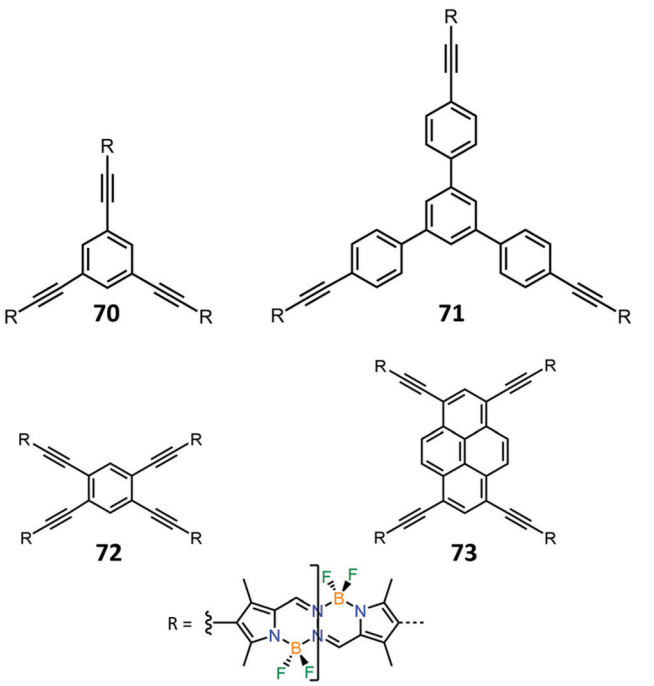

Fig. 17 Molecular structures of BOPHY-based conjugated porous polymers **70–73**.

Table 4 Hydrogen evolution rates and photonic efficiencies under UV-vis illumination of BOPHYs **70–73** and their hybrids with TiO_2[a]

Entry	Photocatalyst	Cocatalyst[b] (wt%)	HER (μmol h^{-1})	Photonic efficiency (%)
1	TiO_2		1.9	0.03
2	Pt/TiO_2	Pt	222.5	3.29
3	**70**	—	2.9	0.04
4	**71**	—	5.6	0.08
5	**72**	—	1.0	0.01
6	**73**	—	4.1	0.06
7	Pt/**70**	Pt	2.9	0.04
8	Pt/**71**	Pt	6.5	0.10
9	Pt/**72**	Pt	1.1	0.02
10	Pt/**73**	Pt	3.8	0.06
11	**70@T-10**	—	24	0.36
12	**71@T-10**	—	5.8	0.09
13	**72@T-10**	—	19.2	0.28
14	**73@T-10**	—	9.6	0.14
15	**70@T-1**	—	4.4	0.07
16	**70@T-5**	—	22.5	0.33
17	**70@T-15**	—	8.3	0.12
18	Pt/**70@T-10**	Pt	982.5	14.54

[a] Reaction conditions: 25 mg of photocatalyst on 130 mL of a methanol aqueous solution (10 vol%) at atmospheric pressure and 20 °C, irradiated by a 150 W medium-pressure Hg immersion lamp. [b] All nominal Pt charges are 1%.

ability of **66** to generate singlet oxygen, a mixture of **66** and DPFB in toluene was irradiated with 500 nm monochromatic light. The intensity of the absorption band at 416 nm was monitored as a function of irradiation time, and it was found to decrease to 80% within six minutes, and completely diminish within 26 minutes (Fig. 15b) with no evidence of photobleaching. These results suggest that **66** is a superior photosensitizer to methylene blue.[31] Employing a water–dimethyl sulfoxide (1 : 1) solution mixture instead of toluene also showed the generation of singlet oxygen, indicating that the process is solvent independent. In a similar vein, Zhao and Zhang studied BOPHY **17** for the purpose of triplet–triplet annihilation upconversion.[101] The authors determined that the triplet state energy level (T_1) of dye **17** lies higher in energy than the T_1 of traditional BODIPY dyes[101–104] suggesting that BOPHYs possessing iodine groups can be promising triplet photosensitizers as well.

In 2015, Ziessel and co-workers synthesized the 3-ethynylperylene bearing dye **67** (Fig. 16a).[62] The incorporation of this group at the 4-position resulted in a strong absorption band with a ε value of 30 000 M^{-1} cm^{-1} in the 400 to 500 nm region (Fig. 16b). Irradiation at 430 nm resulted in very little residual perylene emission (Φ_f = 0.01 at λ_{em} = 515 nm) but strong emission of the BOPHY framework at λ_{em} = 631 nm. These results indicate that an intramolecular cascade energy transfer from the perylene moiety to the dye is occurring with high efficiency, evident by the absence of perylene fluorescence. A significant pseudo-Stokes shift of 5100 cm^{-1} was also observed. Next, Ziessel and coworkers functionalized[105] the BOPHY core at the 3- and 8-positions with vinyl-thiophene groups resulting in dyes **68** and **69** (Fig. 16c). The λ_{max} and ε of these dyes are 595 nm and 626 nm and 97 000 and 11 300 M^{-1} cm^{-1}, respectively, while their Φ_f values were calculated to be 0.13 and 0.10, respectively. Thin films of **68** and **69** gave broadened absorption profiles with a bathochromic shift of 30 nm (Fig. 16d). Next, 1 : 1 mixtures of a fullerene derivative ($PC_{71}BM$) and either **68** or **69** were incorporated into bulk heterojunction solar cells with a small amount of the additive diiodooctane. The average power conversion efficiency for **69** was calculated to be 4.3% (*cf.* 1.5% for **68**) with an external quantum efficiency higher than 70% between 580 to 720 nm. As the first photovoltaic trials using BOPHY dyes – these results are promising for their use in bulk heterojunction solar cells.

In recent work, Liras and O'Shea have successfully used the BOPHY-conjugated porous polymers **70–73** as photocatalysts for hydrogen production (Fig. 17).[106,107] The photocatalytic behavior of **70–73** as well as their hybrid materials with titanium dioxide (calcined PC500) were assessed in the production of hydrogen from water using methanol as a sacrificial agent (Table 4). All of the photocatalytic experiments were performed under UV-vis illumination to ensure that both the polymer and titanium dioxide absorb light. Concurrently, control experiments were carried out in the absence of light to confirm the absence of hydrogen generation. For each system, an estimation of the photonic efficiency (ξ, %) and hydrogen evolution rate (HER) were calculated. All polymers but **72** showed a higher HER and ξ than TiO_2 (Fig. 18b). BOPHY **73** is the most photoactive material

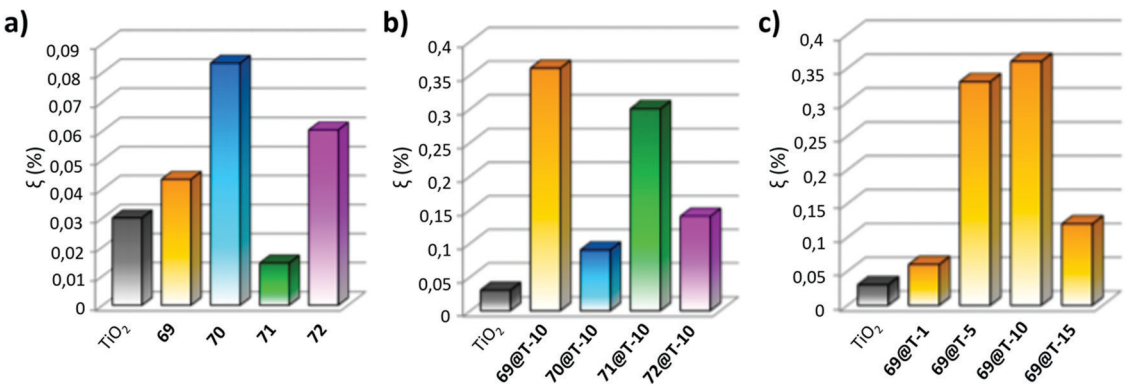

Fig. 18 (a) Comparison of ξ (%) of BOPHY-based conjugated porous polymers used as photocatalysts to TiO_2. (b) ξ (%) of hybrid materials based on TiO_2 and BOPHYs **70–73** at 10 wt% polymer loading. (c) ξ (%) of **70@T** at different loading amounts (1, 5, 10 and 15 wt%). Adapted with permission from ref. 106. Copyright 2020 American Chemical Society.

with hydrogen production three-folds higher than that produced by TiO_2. The photodeposition of 1 wt% platinum (entry 2, Table 4) as cocatalyst boosts the production of hydrogen on titanium dioxide; however, when paired with the BOPHY polymers, **71** and **72** show a marginal increase in hydrogen production whereas **70** and **73** return equal outputs as without any co-catalyst. Hybrid materials composed of TiO_2 and 10 wt% of polymers, named ***x*@T-10** (***x*** = **70**, **71**, **72** or **73**) were also prepared and then assessed as photocatalysts (entries 11–14, Table 4). An increase in ξ was observed in all cases (Fig. 18b). The best performance was observed with **70@T-10**. A study with different amounts of **70** (loading at either 1, 5, 10 or 15 wt%) was then carried out (entries 11 and 15–17, Table 4) and the results (Fig. 18c) demonstrate that ξ continues to increase with the amount of polymer loading until reaching 10%, where a decrease is observed (entry 2 *vs.* entry 18, Table 4). The HER of **70@T-10** was also measured in the presence of photodeposited platinum as cocatalyst (1 wt%). The results display HER which is four-fold higher than that with both platinum and titanium dioxide. Pt/**70@T-10** shows 1.5 and 1.8 times higher HER than the two best systems reported in literature, *i.e.*, truxene-conjugated porous polymer[108] based hybrids. The improved photocatalytic activity is attributed to a type II heterojunction charge transfer mechanism, which has been elucidated by time-resolved fluorescence emission and transient absorption spectroscopy measurements as well as transmission electron microscopy.

5. Conclusions and perspectives

The study of BOPHY fluorophores and their properties has witnessed a surge since their first inception in 2014. This emerging family of BF_2-based dyes are easily accessible, yielding a wide variety of derivatives through substitution at the α- and β-position(s). There are two main synthetic pathways to accomplish such modifications, the first one involving a key Knoevenagel condensation reaction as described in Scheme 1. Here, the desired functionality is either already installed on the pyrrole precursor or is introduced in later steps through appropriate transformations. The second key method involves the introduction of halogen(s) to the core, followed by a palladium-catalyzed cross-coupling reaction to give the desired BOPHY derivative. Although there has been great success with substitution at the α- and β-position(s) of the BOPHY core, derivatives substituted at the *meso*-position are lacking, largely because of the instability of such compounds.[71] The variety of functional groups that can be attached to the BOPY core are also somewhat limited. For example, ferrocene is the only organometallic compound to be attached to the BOPHY core. Moreover, this fluorophore is yet to be incorporated into attractive architectures such as cages, macrocycles, liquid crystals, or metal–organic frameworks. On the other hand, several organometallic-based BODIPYs have been prepared and studied (*e.g.*, BODIPY-based Ru^{2+} and Ir^{2+} complexes)[109] and BODIPY-based photocages[110] and macrocycles[111] have been investigated. Considering the fast pace at which this family of dyes is being developed, headways in these directions seems inevitable.

The tuning of pivotal (photo)physical properties through careful synthetic modifications has been vital not only for the development of applications – in research fields ranging from biology to materials chemistry – but also in gaining important fundamental understanding of the parameters that control the photophysical properties of the dyes. The appealing photophysical properties of the BOPHY dyes include high fluorescence quantum yields – some of which approach near unity – large molar extinction coefficients, as well as tunable absorption and emission maxima. The BOPHY chromophores also exhibit reasonable resistance to photo-degradation, but autocatalysis is observed such that the rate of degradation escalates with increasing exposure time.[112] Moreover, the dyes typically display fluorescence emission in the solid state – a property which BODIPY dyes struggle with. Fusing the core with either a benzene, thiophene or furan ring is another method of drastically altering the properties of the dyes and achieving a significant bathochromic shift in absorption and emission bands. Although only modest Φ_f values (0.22–0.64) are obtained from these fused systems, they exhibit some of the largest red shifts in absorption and emission bands, 182 and 174 nm respectively compared to the parent system **8**. Further to this, the furan-BOPHYs (**30**–**32**) also boast high ε values. Other adaptations to the BOPHY chromophore result in moderate changes to the photophysical properties, although interesting properties in specific systems have been uncovered in some cases, such as metal-to-ligand charge-transfer and aggregation-induced emission enhancement. ICT has continuously shown to reduce quantum yields in these dyes, which is an issue that must be tackled when designing systems for luminescent applications.

While relatively new on the scene, BOPHY fluorophores have already been used in numerous applications spanning many research areas. The pH-sensitivity of the fluorescence intensity in certain dyes was used in measuring the pH changes within cells. Such changes are biomarkers for diverse physiological processes such as cell proliferation[113] and apoptosis.[114] To be used in monitoring such processes though the dyes need to be made more biocompatible and water soluble. The latter can be accomplished by introducing water solubilizing groups – something which is yet to be accomplished with BOPHY dyes. Cell imaging has also been demonstrated with BOPHY dyes as either part of CNPs or when functionalized with an azine group, allowing for the sensing of Cu^{2+} ions. The former systems, which possess good stability as well as low toxicity, emit in the far-red and NIR region and can be used in imaging HeLa cells. Sensing of Cu^{2+} ions with the latter motif was shown to be selective and sensitive within diluted human serum samples and living HeLa cells. In another study, a dye was used in selectively sensing Cd^{2+} ions,[97] showing the scope for BOPHYs in the recognition of a range of ions. Further optimization of the dyes is needed for their use in *in vivo* studies. On this note, some progress has already been achieved with an improvement in the detection limit of the Cu^{2+} sensor from 50 to 1 nM over a period of two years.

Halogenated BOPHYs developed as photosensitizers for singlet oxygen generation demonstrate fast production of singlet oxygen with no photobleaching.[115] This property opens the way for using the dyes in photodynamic therapy, photocatalysis and water purification.[116] Addition of vinyl-thiophene modules at the 3- and 8-positions allows for the use of the dyes in bulk heterojunction solar cells, with an average power conversion efficiency of 4.3%. Given this preliminary study, there is great potential for further optimization and improvement of these values. Conjugated polymers based on the BOPHY motif have also proven viable as photocatalysts for hydrogen production. Hybrids of these polymers with TiO_2 show improved photocatalytic activity with photonic efficiencies over four-fold higher than that of Pt/TiO_2. The improved photocatalytic activity is attributed to a type II heterojunction charge transfer mechanism. Currently, these systems harness UV-vis radiation. Future improvements should look into exploiting visible light, a significant component of solar energy, for maximum benefit.

In this review, we have sought to outline the key synthetic strategies used in the preparation of BOPHY dyes, while drawing attention to the effect of different functional groups on the photophysical properties. We also showcased some promising applications the dyes can be used in (*i.e.*, biosensing).[117] Whilst the BOPHY moiety itself is relatively new and some initial progress has been made in diversifying the dyes scaffold, a greater variety in structural modification must be explored, to take advantage of the full potential of this new class of dyes. Research in this area has already spurred new dye scaffolds such as BOPPY,[118] which encompasses both pyrrole and *N*-heteroarene derivatives, and BOPYPY,[119] which is a pyrazine-pyrrole fused system. Considering all the progress with these dyes and their swift adaptation – it is clear that the BOPHY dyes have a bright future.

Author contributions

A. N. B. and I. A. conceptualized the topics, prepared, and edited the manuscript.

Conflicts of interest

There are no conflicts to declare.

Acknowledgements

The authors acknowledge the US–UK Fulbright Commission and the National Science Foundation (CHE-1807428) for their generous support.

References

1 S. M. Sentha and N. M. Shah, *Chem. Rev.*, 1945, **36**, 1–62.
2 M. Oelgemöller and W. H. Kramer, *J. Photochem. Photobiol., C*, 2010, **11**, 210–244.
3 R. Sjöback, J. Nygren and M. Kubista, *Spectrochim. Acta, Part A*, 1995, **51**, L7–L21.
4 H. Zheng, X.-Q. Zhan, Q.-N. Bian and X.-J. Zhang, *Chem. Commun.*, 2013, **49**, 429–447.
5 M. R. Wasielewski, *Chem. Rev.*, 1992, **92**, 435–461.
6 M. Beija, C. A. M. Afonso and J. M. G. Martinho, *Chem. Soc. Rev.*, 2009, **38**, 2410–2433.
7 L. Beverina and P. Salice, *Eur. J. Org. Chem.*, 2010, 1207–1225.
8 T. Weil, T. Vosch, J. Hofkenes, K. Peneva and K. Müllen, *Angew. Chem., Int. Ed.*, 2010, **49**, 9068–9093.
9 A. Loudet and K. Burgess, *Chem. Rev.*, 2007, **107**, 4891–4932.
10 G. Ulrich, C. Goze, M. Guardigli, A. Roda and R. Ziessel, *Angew. Chem., Int. Ed.*, 2005, **44**, 3694–3698.
11 S. Hapuarachchige, G. Montaño, C. Ramesh, D. Rodriguez, L. H. Henson, C. C. Williams, S. Kadavakkollu, D. L. Johnson, C. B. Shuster and J. B. Arterburn, *J. Am. Chem. Soc.*, 2011, **133**, 6780–6790.
12 A. Vázquez-Romero, N. Kielland, M. J. Arévalo, S. Preciado, R. J. Mellanby, Y. Feng, R. Lavilla and M. Vendrell, *J. Am. Chem. Soc.*, 2013, **135**, 16018–16021.
13 Y. Hong, J. W. Y. Lam and B. Z. Tang, *Chem. Soc. Rev.*, 2011, **40**, 5361–5388.
14 Z. Chi, X. Zhang, B. Xu, X. Zhou, C. Ma, Y. Zhang, S. Liu and J. Xu, *Chem. Soc. Rev.*, 2012, **41**, 3878–3896.
15 H. Zheng, X.-Q. Zhan, Q.-N. Bian and X.-J. Zhang, *Chem. Commun.*, 2013, **49**, 429–447.
16 H. Maeda and Y. Bando, *Chem. Commun.*, 2013, **49**, 4100–4113.
17 M. Oelgemöller and W. H. Kramer, *J. Photochem. Photobiol., C*, 2010, **11**, 210–244.
18 A. Hagfeldt, G. Boschloo, L. Sun, L. Kloo and H. Pettersson, *Chem. Rev.*, 2010, **110**, 6595–6663.
19 S. Reineke, F. Lindner, G. Schwartz, N. Seidler, K. Walzer, B. Lussem and K. Leo, *Nature*, 2009, **459**, 234–238.
20 Q. Zhang, J. Li, K. Shizu, S. Huang, S. Hirata, H. Miyazaki and C. Adachi, *J. Am. Chem. Soc.*, 2012, **134**, 14706–14709.
21 D. Li, H. Zhang and Y. Wang, *Chem. Soc. Rev.*, 2013, **42**, 8416–8433.
22 J. Mei, N. L. Leung, R. T. K. Kwok, J. W. Y. Lam and B. Z. Tang, *Chem. Rev.*, 2015, **115**, 11718–11940.
23 L. Zhang, *Acc. Chem. Res.*, 2015, **48**, 2705–2714.
24 H. Mustroph, M. Stollenwerk and V. Bressau, *Angew. Chem., Int. Ed.*, 2006, **45**, 2016–2035.
25 K. Rurack, M. Kollmannsberger and J. Daub, *Angew. Chem., Int. Ed.*, 2001, **40**, 385–387.
26 K. Y. Law, *Chem. Rev.*, 1993, **93**, 449–486.
27 W. Pham, R. Weissleder and C.-H. Tung, *Angew. Chem., Int. Ed.*, 2002, **41**, 3659–3662.
28 E. Sasaki, H. Kojima, H. Nishimatsu, Y. Urano, K. Kikuchi, Y. Hirata and T. Nagano, *J. Am. Chem. Soc.*, 2005, **127**, 3684–3685.
29 V. Ntziachristos, J. Ripoll, L. H. V. Wang and R. Weissleder, *Nat. Biotechnol.*, 2005, **23**, 313–320.
30 J. Killoran, L. Allen, J. F. Gallagher, W. M. Gallagher and D. F. O'Shea, *Chem. Commun.*, 2002, 1862–1863.
31 A. Gorman, J. Killoran, C. O'Shea, T. Kenna, W. M. Gallagher and D. F. O'Shea, *J. Am. Chem. Soc.*, 2004, **126**, 10619–10631.

32 S. O. McDonnell, M. J. Hall, L. T. Allen, A. Bryne, W. M. Gallagher and D. F. O'Shea, *J. Am. Chem. Soc.*, 2005, **127**, 16360–16361.
33 J. Murtagh, D. O. Frimannsson and D. F. O'Shea, *Org. Lett.*, 2009, **11**, 5368–5389.
34 R. E. Gawley, H. Mao, M. M. Haque, J. B. Thorne and J. S. Pharr, *J. Org. Chem.*, 2007, **72**, 2187–2191.
35 A. Palma, M. Tasior, D. O. Frimannsson, T. T. Vu, R. Méallet-Renault and D. F. O'Shea, *Org. Lett.*, 2009, **11**, 3638–3641.
36 N. Boens, V. Leen and W. Dehaen, *Chem. Soc. Rev.*, 2012, **41**, 1130–1172.
37 C. Yu, X. Fang, Q. Wu, L. Jiao, L. Sun, Z. Li, P.-K. So, W.-Y. Wong and E. Hao, *Org. Lett.*, 2020, **22**, 4588–4592.
38 C. Yu, L. Jiao, P. Zhang, Z. Feng, C. Cheng, Y. Wei, X. Mu and E. Hao, *Org. Lett.*, 2014, **16**, 3048–3051.
39 T. T. Vu, S. Badré, C. Dumas-Verdes, J. J. Vachon, C. Julien, P. Audebert, E. Y. Senotrysova, E. Y. Schmidt, B. A. Trofimov, R. B. Pansu, G. Clavier and R. Méallet-Renault, *J. Phys. Chem. C*, 2009, **113**, 11844–11855.
40 T. Ozdemir, S. Atilgan, I. Kutuk, L. T. Yildrim, A. Tulek, M. Bayindir and E. U. Akkaya, *Org. Lett.*, 2009, **11**, 2105–2107.
41 Y. Yang, X. Su, C. N. Carroll and I. Aprahamian, *Chem. Sci.*, 2012, **3**, 610–613.
42 Z. Shi, X. Han, W. Hu, H. Bai, B. Peng, L. Ji, Q. Fan, L. Li and W. Huang, *Chem. Soc. Rev.*, 2020, **49**, 7533–7567.
43 Y. Xu, M. Zhao, L. Zou, L. Wu, M. Xie, T. Yang, S. Liu, W. Huang and Q. Zhao, *ACS Appl. Mater. Interfaces*, 2018, **10**, 44324–44335.
44 Y. Kage, S. Mori, M. Ide, A. Saeki, H. Furuta and S. Shimizu, *Mater. Chem. Front.*, 2018, **2**, 112–120.
45 W. Sheng, Y. Wu, C. Yu, P. Bobadova-Parvanova, E. Hao and L. Jiao, *Org. Lett.*, 2018, **20**, 2620–2623.
46 H. Qian, M. E. Cousins, E. H. Horak, A. Wakefield, M. D. Liptak and I. Aprahamian, *Nat. Chem.*, 2017, **9**, 83–87.
47 J. F. Araneda, W. E. Piers, B. Heyne, M. Parvez and R. M. McDonald, *Angew. Chem., Int. Ed.*, 2011, **50**, 12214–12217.
48 S. Mula, N. Leclerc, P. Lévêque, R. Retailleau and G. Ulrich, *J. Org. Chem.*, 2018, **83**, 14406–14418.
49 L. J. Patalag, P. G. Jones and D. B. Werz, *Angew. Chem., Int. Ed.*, 2016, **55**, 13340–13344.
50 J. Patalag, P. G. Jones and D. B. Werz, *Chem. – Eur. J.*, 2017, **23**, 15903–15907.
51 G. Nawn, S. R. Oakley, M. B. Majewski, R. McDonald, B. O. Patrick and R. G. Hicks, *Chem. Sci.*, 2013, **4**, 612–621.
52 D. Frath, S. Azizi, G. Ulrich and R. Ziessel, *Org. Lett.*, 2012, **14**, 4774–4777.
53 S. P. Parambil, F. de Jong, K. Veys, J. Huang, S. P. Veettil, D. Verhaeghe, L. V. Meervelt, D. Escudero, M. V. der Auweraer and W. Dehaen, *Chem. Commun.*, 2020, **56**, 5791–5794.
54 C. Yu, E. Hao, X. Fang, Q. Wu, L. Wang, J. Li, L. Xu, L. Jiao and W.-Y. Wong, *J. Mater. Chem. C*, 2019, **7**, 3269–3277.
55 I.-S. Tamgho, A. Hasheminasab, J. T. Engle, V. N. Nemykin and C. J. Ziegler, *J. Am. Chem. Soc.*, 2014, **136**, 5623–5626.
56 S. Boodts, E. Fron, J. Hofkens and W. Dehaen, *Coord. Chem. Rev.*, 2018, **371**, 1–10.
57 R. Sola-Llano, J. Jiménez, E. Avellanal-Zaballa, M. Johnson, T. A. Cabreros, F. Moreno, B. L. Maroto, G. Muller, J. Bañuelos, L. Cerdán, I. García-Moreno and S. de la Moya, *Dyes Pigm.*, 2019, **170**, 107662.
58 X. Li, G. Ji and Y.-A. Son, *Dyes Pigm.*, 2016, **124**, 232–240.
59 M. Zhang, E. Hao, Y. Xu, S. Zhang, H. Zhu, Q. Wang, C. Yu and L. Jiao, *RSC Adv.*, 2012, **2**, 11215–11218.
60 L. Wang, I.-S. Tamgho, L. A. Crandall, J. J. Rack and C. J. Ziegler, *Phys. Chem. Chem. Phys.*, 2015, **17**, 2349–2351.
61 X. Lv, T. Li, Q. Wu, C. Yu, L. Jiao and E. Hao, *J. Org. Chem.*, 2018, **83**, 1134–1145.
62 Q. Huaulme, A. Mirlop, P. Retailleau and R. Ziessel, *Org. Lett.*, 2015, **17**, 2246–2249.
63 S. Boodts, J. Hofkens and W. Dehaen, *Dyes Pigm.*, 2017, **142**, 249–254.
64 X. Li, G. Ji and Y.-A. Son, *Dyes Pigm.*, 2015, **124**, 232–240.
65 J. Wang, Q. Wu, C. Yu, Y. Wei, X. Mu, E. Hao and L. Jiao, *J. Org. Chem.*, 2016, **81**, 11316–11323.
66 A. Wakamiya, T. Murakami and S. Yamaguchi, *Chem. Sci.*, 2013, **4**, 1002–1007.
67 L. Zhou, D. Xu, H. Gao, C. Zhang, F. Ni, W. Zhao, D. Cheng, X. Liu and A. Han, *J. Org. Chem.*, 2016, **81**, 7439–7477.
68 H. M. Rhoda, K. Chanawanno, A. J. King, Y. V. Zatsikha, C. J. Ziegler and V. N. Menykin, *Chem. – Eur. J.*, 2015, **21**, 18043–18046.
69 O. J. Woodford, P. Stachelek, R. Ziessel, N. Algoazy, J. G. Knight and A. Harriman, *New J. Chem.*, 2018, **42**, 4835–4842.
70 Y. V. Zatsikha, D. B. Nemez, R. L. Davis, S. Singh, D. E. Herbert, A. J. King, C. J. Ziegler and V. N. Menykin, *Chem. – Eur. J.*, 2017, **23**, 14786–14796.
71 Y. V. Zatsikha, E. Maligaspe, A. A. Purchel, N. O. Didukh, Y. Wang, Y. P. Kovtun, D. A. Blank and V. N. Menykin, *Inorg. Chem.*, 2015, **54**, 7915–7928.
72 T. Rohand, M. Brauah, W. Qin, N. Boens and W. Dehaen, *Chem. Commun.*, 2006, 266–268.
73 T. Jiang, P. Zhang, C. Yu, J. Yin, L. Jiao, E. Dai, J. Wang, X. Mu and E. Hao, *Org. Lett.*, 2014, **16**, 1952–1955.
74 V. Lakshmi, M. R. Rao and M. Ravikanth, *Org. Biomol. Chem.*, 2015, **13**, 2501–2517.
75 N. Zhao, S. Xuan, F. R. Fronczek, M. K. Smith and M. G. H. Vicente, *J. Org. Chem.*, 2015, **80**, 8377–8383.
76 Z. Feng, L. Jiao, Y. Feng, C. Yu, N. Chen, Y. Wei, X. Mu and E. Hao, *J. Org. Chem.*, 2016, **81**, 6281–6291.
77 L. Jiang, H. Gao, L. Gai and Z. Shen, *New J. Chem.*, 2018, **42**, 8271–8275.
78 F. Würthner, T. E. Kaiser and C. R. Saha-Möller, *Angew. Chem., Int. Ed.*, 2011, **50**, 3376–3410.
79 Y. Hayashi, S. Yamaguchi, W. Y. Cha, D. Kim and H. Shinokubo, *Org. Lett.*, 2011, **13**, 2992–2995.
80 F. Li, S. I. Yang, Y. Ciringh, J. Seth, C. H. Martin, D. L. Singh, D. Kim, R. R. Birge, D. F. Bocian, D. Holten and J. S. Lindsey, *J. Am. Chem. Soc.*, 1998, **120**, 10001–10017.
81 J. Zhao, K. Xu, W. Yang, Z. Wang and F. Zhong, *Chem. Soc. Rev.*, 2015, **44**, 8904–8939.

82 M. Más-Montoya and R. A. J. Janssen, *Adv. Funct. Mater.*, 2017, **27**, 1605779.
83 J. Mei, N. L. C. Leung, R. T. K. Kwock, J. W. Y. Lam and B. Z. Tang, *Chem. Rev.*, 2015, **115**, 11718–11940.
84 W. Cooper, *Chem. Phys. Lett.*, 1970, **7**, 73–77.
85 X.-D. Jiang, Y. Su, S. Yue, C. Li, H. Yu, H. Zhang, C.-L. Sun and L.-J. Xiao, *RSC Adv.*, 2005, **5**, 16735–16739.
86 Y. Chen, D. Qi, L. Zhao, W. Cao, C. Huang and J. Jiang, *Chem. – Eur. J.*, 2013, **23**, 7342–7437.
87 C. Thivierge, J. Han, R. M. Jenkins and K. Burgess, *J. Org. Chem.*, 2011, **76**, 5129–5288.
88 C. Dai, D. Yang, W. Zhang, B. Bao, Y. Cheng and L. Wang, *Polym. Chem.*, 2015, **6**, 3962–3969.
89 J. Pecher and S. Mecking, *Chem. Rev.*, 2010, **110**, 6260–6279.
90 Y. Li, H. Zhou, S. Yin, H. Jiang, N. Niu, H. Huang, S. A. Shahzad and C. Yu, *Sens. Actuators, B*, 2016, **235**, 33–38.
91 E. Karakus, M. Ucunncu and M. Emrullahoglu, *Chem. Commun.*, 2014, **50**, 1119–1121.
92 M. Ucunncu and M. Emrullahoglu, *Chem. Commun.*, 2014, **50**, 5884–5886.
93 L. Y. Niu, Y. S. Guan, Y. Z. Chen, L. Z. Wu, C. H. Tung and Q. Z. Yang, *J. Am. Chem. Soc.*, 2012, **134**, 18928–18931.
94 J. Zhang, B. Zhao, C. Li, X. Zhu and R. Qiao, *Sens. Actuators, B*, 2014, **196**, 117–122.
95 J.-H. Ye, J. Xu, H. Chen, Y. Bai, W. Zhang and W. He, *RSC Adv.*, 2014, **4**, 6691–6695.
96 M.-Q. Wang, K. Li, I.-T. Hou, M.-Y. Wu, Z. Huang and X.-Q. Yu, *J. Org. Chem.*, 2012, **77**, 8350–8354.
97 C. He, H. Zhou, N. Yang, N. Niu, E. Hussain, Y. Li and C. Yu, *New J. Chem.*, 2018, **42**, 2520–2525.
98 D. Cheng, X. Liu, Y. Xie, H. Lv, Z. Wang, H. Yang, A. Han, X. Yang and L. Zang, *Sensors*, 2017, **17**, 2517–2527.
99 T.-F. Cui, J. Zhang, X.-D. Jiang, Y.-S. Su, C.-L. Sun and J.-L. Zhao, *Chin. Chem. Lett.*, 2016, **27**, 190–194.
100 T. Jiang, P. Zhang, C. Yu, J. Yin, L. Jiao, E. Dai, J. Wang, Y. Wei, X. Mu and E. Hao, *Org. Lett.*, 2014, **16**, 1952–1955.
101 C. Zhang and J. Zhao, *J. Mater. Chem. C*, 2016, **4**, 1623–1632.
102 Z. Wang, Y. Xie, K. Xu, J. Zhao and K. D. Glusac, *J. Phys. Chem. A*, 2015, **119**, 6791–6806.
103 S. Wu, F. Zhong, J. Zhao, S. Guo, W. Yang and T. Fyles, *J. Phys. Chem. A*, 2015, **119**, 4787–4799.
104 Z. Mahood, K. Xu, B. Kücüköz, X. Cui, J. Zhao, Z. Wang, A. Karatay, H. G. Yaglioglu, M. Hayvali and A. Elmali, *J. Org. Chem. A*, 2015, **80**, 3036–3049.
105 A. Mirloup, Q. Huaulmé, N. Leclerc, P. Lévêque, T. Heiser, P. Retailleau and R. Ziessel, *Chem. Commun.*, 2015, **51**, 14742–14745.
106 C. G. López-Calixto, M. Barawl, M. Gomez-Mendoza, F. E. Oropeza, F. Fresno, M. Liras and V. A. de la Peña O'Shea, *ACS Catal.*, 2020, **10**, 9804–9812.
107 C. G. López-Calixto, S. Cabrera, R. Pérez-Ruiz, M. Barawi, J. Alemàn, V. A. de la Peña O'Shea and M. Liras, *Appl. Catal., B*, 2019, **258**, 117933.
108 A. Valverde-González, C. G. López Calixto, M. Barawi, M. Gomez-Mendoza, V. A. de la Peña O'Shea, M. Liras, B. Gómez-Lor and M. Iglesias, *ACS Appl. Energy Mater.*, 2020, **3**, 4411–4420.
109 G. Gupta, S. Cherukommu, G. Srinivas, S. W. Lee, S. H. Mun, J. Jung, N. Nagesh and C. Y. Lee, *J. Inorg. Biochem.*, 2018, **189**, 17–29.
110 D. Kand, P. Liu, M. X. Navarro, L. J. Fischer, L. Rousso-Norri, D. Friedmann-Morvinski, A. H. Winter, E. W. Miller and R. Weinstain, *J. Am. Chem. Soc.*, 2020, **142**, 4970–4974.
111 Y. Qin, X. Liu, P.-P. Jia, L. Xu and J.-B. Yang, *Chem. Soc. Rev.*, 2020, **49**, 5678–5703.
112 O. J. Woodford, A. Harriman, W. McFarlane and C. Wills, *ChemPhotoChem*, 2017, **1**, 317–326.
113 M. Flink, S. H. Kramer and S. F. Pederson, *Acta Physiol.*, 2018, **223**, e13068.
114 D. Lagadic-Gossmann, L. Huc and V. Leecurer, *Cell Death Differ.*, 2004, **11**, 953–961.
115 J. P. Tardivo, A. D. Giglio, C. S. de Oliveria, D. S. Gabrielli, H. C. Junqueria, D. B. Tada, D. Severino, R. F. Turchiello and M. S. Baptista, *Photodiagn. Photodyn. Ther.*, 2005, **2**, 175–191.
116 D. Beri, M. Jakoby, D. Busko, B. S. Richards and A. Turshatov, *Front. Chem.*, 2020, **5**, 567.
117 M. Ponce-Vargas, C. Azarias, D. Jacquemin and B. Le Guennic, *J. Phys. Chem. B*, 2017, **121**, 10850–10858.
118 X. Jiang, S. Yue, K. Chen, Z. Shao, C. Li, Y. Su and J. Zhao, *Chin. Chem. Lett.*, 2019, **30**, 2271–2273.
119 C. Yu, Z. Huang, X. Wang, Q. Miao, Q. Wu, W.-Y. Wong, E. Hao, Y. Xiao and L. Jiao, *Org. Lett.*, 2018, **20**, 4462–4466.